RESEARCH ARTICLE

ATP8B1–TMEM30B flippase activity maintains stereocilia lipid asymmetry required for hearing

Henry Newkirk De Hoyos[1,2,3], Sihan Li[1], Jun-Sub Im[1], Alyssa Luz-Ricca[1], Takesha Foster[1], Betsy Szeto[4], Rachel Jonas[4], Emma Kim[1], Nikhil Amin[1], Jung-Bum Shin[1,2,4,5,6]*

[1]Departments of Neuroscience, School of Medicine, University of Virginia, Charlottesville, United States; [2]Biochemistry and Molecular Genetics, School of Medicine, University of Virginia, Charlottesville, United States; [3]Medical Scientist Training Program, School of Medicine, University of Virginia, Charlottesville, United States; [4]Otolaryngology-Head and Neck Surgery, School of Medicine, University of Virginia, Charlottesville, United States; [5]Cell Biology, School of Medicine, University of Virginia, Charlottesville, United States; [6]Membrane and Cell Physiology, School of Medicine, University of Virginia, Charlottesville, United States

***For correspondence:** js2ee@virginia.edu

Competing interest: The authors declare that no competing interests exist.

Funding: See page 19

Preprint posted
13 February 2026
Sent for Review
11 February 2026
Reviewed preprint v1
02 April 2026
Reviewed preprint v2
26 August 2026
Reviewed preprint v3
09 November 2026
Version of Record
23 November 2026

Reviewing Editor: Doris K Wu, National Institutes of Health, United States

© Copyright De Hoyos *et al*. This article is distributed under the terms of the Creative Commons Attribution License, which permits unrestricted use and redistribution provided that the original author and source are credited.

eLife Assessment

Mechanical transduction channels of sensory hair cells possess lipid scramblase activity. Membrane lipid disruption resulting from mechanical transduction is thought to be restored by flippase activities. This **fundamental** study provides **compelling** evidence that ATP8B1, a P4-ATP flippase and its subunit TMEM30B, are key in mediating this restorative function in outer hair cells of the mammalian cochlea.

Abstract Sensory hair cells convert sound-induced vibrations into electrical signals through a process called mechano-electrical transduction (MET). While the protein components of the MET complex are well studied, increasing evidence indicates that MET channel properties are significantly modulated by the surrounding lipid bilayer. The asymmetric distribution of membrane lipids between the inner and outer membrane leaflets is well established to shape membrane mechanics. The recent discovery that the core MET components TMC1 and TMC2 also act as lipid scramblases suggests a direct role for membrane lipid asymmetry in the dynamic shaping of auditory transduction. Because scramblase activity of TMC1/2 disrupts lipid asymmetry, we hypothesized that an opposing flippase may be required to restore and maintain lipid asymmetry. Here, we identify the P4-ATPase ATP8B1 and its chaperone TMEM30B as selectively expressed in mouse outer hair cells (OHCs), enriched in stereocilia, and upregulated following the onset of MET and hearing. Loss of either protein results in elevated auditory brainstem response (ABR) thresholds, phosphatidylserine (PS) externalization, and rapid hair-cell degeneration, demonstrating that lipid homeostasis is crucial for OHC survival. Together, these findings establish ATP8B1 and TMEM30B as key regulators of membrane lipid asymmetry in sensory hair cells and establish TMEM30B as a novel deafness gene.

Introduction

Hearing depends on the ability of mechanosensory hair cells to convert sound-evoked mechanical forces into electrical signals (**Hudspeth, 1989**; **Gillespie and Müller, 2009**; **Fettiplace and Kim, 2014**). Sound vibrations transmitted through the middle ear displace the basilar membrane and deflect the stereocilia bundles that crown auditory hair cells. This deflection modulates tension on tip links, which are filamentous connectors that couple adjacent stereocilia and directly gate mechanotransduction (MET) channels. The architecture of the hair bundle, including the graded heights of stereocilia rows and the polarity of the MET machinery, is essential for tuning the sensitivity and dynamic range of auditory signaling. Many of the protein components of the MET complex have now been identified. At the core of this machinery is a force-transmission complex that couples the extracellular tip link to the MET channel complex. Tip links are formed by cadherin 23 and protocadherin 15 (**Pickles et al., 1984**; **Assad et al., 1991**; **Siemens et al., 2004**; **Kazmierczak et al., 2007**; **Ahmed et al., 2006**), which relay mechanical force to the MET channel through a network of associated proteins, including LHFPL5 (**Xiong et al., 2012**), CIB2 (**Riazuddin et al., 2012**; **Giese et al., 2017**), and TMIE (**Zhao et al., 2014**). TMC1 and its paralog TMC2 are proposed to constitute the ion-conducting components of the MET channel, with TMC1 serving as the dominant pore-forming subunit in mature mammalian hair cells (**Kawashima et al., 2011**; **Pan et al., 2013**; **Pan et al., 2018**; **Assad et al., 1991**; **Pickles et al., 1984**). Intriguingly, TMC1 and TMC2 share structural similarity with TMEM16 family lipid scramblases, of which TMEM16A and TMEM16B function as ion channels (**Le and Yang, 2021**). More broadly, TMEM16, TMC, and TMEM63/OSCA are members of a structurally related superfamily of membrane proteins that includes ion channels and lipid scramblases (**Medrano-Soto et al., 2018**). Consistent with this relationship, TMC1 and TMC2 were shown to possess lipid-scrambling activity in addition to their proposed ion-conducting function (**Ballesteros et al., 2018**; **Ballesteros and Swartz, 2022**; **Clark et al., 2024**; **Peineau et al., 2025**; **George and Ricci, 2026**). Cryo-EM structures of *C. elegans* homologues of TMC1 reveal that TMC1 forms a dimer associated with TMIE and calcium-binding accessory proteins and engages extensively with the surrounding lipid bilayer (**Jeong et al., 2022**; **Clark et al., 2024**). These structures resolve conserved lipid-like densities at defined positions around the complex, including a lipid-filled cavity at the TMIE–TMC interface and sterol-like densities near the dimer interface (**Jeong et al., 2022**; **Clark et al., 2024**). Such lipid-mediated interactions appear to stabilize subunit assembly and may influence conformational changes during channel gating. Together, these findings suggest that the membrane is an active component of the MET complex, with lipid–protein interactions poised to shape MET properties, including sensitivity, resting open probability, and adaptation.

These observations further imply that MET function may require a specialized lipid environment within stereocilia, whose composition and organization are distinct from the surrounding apical membrane. However, the molecular mechanisms, including the lipid-modifying enzymes, transport pathways, and regulatory factors, that establish, maintain, and dynamically regulate this unique lipid milieu are unknown.

Lipids are not uniformly distributed across the plasma membrane (**Bretscher, 1972**). Instead, eukaryotic membranes maintain a highly asymmetric distribution of phospholipids between their inner and outer leaflets (**Cooper, 2000**; **Lorent et al., 2020**). Phosphatidylserine (PS) and phosphatidylethanolamine (PE) are normally enriched on the cytoplasmic leaflet, whereas phosphatidylcholine (PC) and sphingomyelin predominate externally (**Cooper, 2000**; **Lorent et al., 2020**). This asymmetry is actively maintained by ATP-dependent flippases and floppases and disrupted by scramblases (**Nagata et al., 2020**).

Possibly best studied is the asymmetric distribution of PS. Loss of PS asymmetry is widely recognized as a potent cellular signal, as PS is normally confined to the cytoplasmic leaflet by ATP-dependent flippases (**Nagata et al., 2020**). Its externalization is best known as a hallmark of apoptosis, where it functions as an 'eat-me' signal that promotes rapid clearance of dying cells (**Nagata et al., 2010**; **Suzuki et al., 2010**). However, PS exposure is not exclusively associated with cell death. In immune cells and platelets, transient PS externalization accompanies physiological activation states and serves signaling or catalytic roles, illustrating that regulated loss of asymmetry can be functionally repurposed (**Shin and Takatsu, 2020**). PS exposure has also been implicated in cell–cell fusion events, where localized scrambling appears to facilitate membrane remodeling and lower energetic barriers to cell–cell fusion (**Whitlock and Chernomordik, 2021**).

Beyond signaling, lipid asymmetry has significant biophysical consequences for the membrane. Asymmetric enrichment of charged, unsaturated lipids such as PS and PE in the inner leaflet, opposed by PC, sphingomyelin-, and cholesterol-rich outer leaflets, creates differences in lipid packing, order, and viscosity across the bilayer (**Reddy et al., 2012**; **Hossein and Deserno, 2020**; **Doktorova et al., 2020**; **Kakuda et al., 2022**; **Li et al., 2024**; **Wang et al., 2025**). This asymmetry strongly influences membrane tension, curvature stress, and bending rigidity, parameters that govern how membranes deform and how embedded proteins respond to force (**Lorent et al., 2020**; **Hossein and Deserno, 2020**; **Wang et al., 2025**).

In this context, the scramblase activity associated with TMC proteins raises an important question: does TMC-mediated lipid scrambling represent an unintended byproduct of MET, or does it serve a specific functional role? Initial models proposed that scrambling might facilitate adaptive membrane remodeling or ectosome shedding (**Ballesteros and Swartz, 2022**). Given the exquisite sensitivity of MET channel function to the surrounding lipid environment, it is also hypothesized that regulated scrambling directly modulates MET gating by altering membrane mechanical properties (**George and Ricci, 2026**). Regardless of its precise physiological benefit, sustained lipid scrambling would be incompatible with cellular homeostasis, as aberrant PS exposure and loss of membrane asymmetry are broadly harmful for the cell (**Ballesteros and Swartz, 2022**; **Beurg et al., 2025**). Thus, mechanisms that actively restore lipid asymmetry are likely essential in hair cells.

P4-ATPases, the canonical phospholipid flippases, are prime candidates for maintaining this asymmetry (**Segawa et al., 2016**). These enzymes selectively transport PS and other phospholipids from the outer to the inner leaflet and require CDC50 family accessory subunits (also known as TMEM30A, TMEM30B, and TMEM30C) for proper folding, trafficking, and activity (**Lenoir et al., 2009**; **Bryde et al., 2010**; **van der Velden et al., 2010**; **Segawa et al., 2018**; **Figure 1A**). While TMEM30A is ubiquitously expressed and supports multiple P4-ATPases, TMEM30B exhibits more restricted tissue distribution and remains poorly characterized (**Segawa et al., 2018**; **Li et al., 2021**; **Xing et al., 2023**). TMEM30C is known to only be expressed in mammalian testis (**Osada et al., 2007**). Transcriptomic analyses indicate that TMEM30B is expressed in the inner ear (**Liu et al., 2018**; **Scheffer et al., 2015**; **Kolla et al., 2020**; **Orvis et al., 2021**), and a recent hearing loss screen in a cohort of 3006 mouse knockout (KO) strains reported that *Tmem30b* KO mice develop hearing loss (**Bowl et al., 2017**). However, the cellular and molecular basis of the hearing loss, and the developmental regulation and subcellular localization of TMEM30B in hair cells remained unknown.

Here, we investigate the roles of the flippase ATP8B1 and its accessory subunit TMEM30B in auditory hair cells. We show that both proteins are highly enriched in stereocilia and the apical membrane. Using genetic KO mouse models, we demonstrate that loss of ATP8B1 leads to loss of lipid membrane asymmetry, early-onset hair cell pathology, and rapid hearing decline. *Tmem30b* KO mice phenocopy these defects. Together, our findings identify ATP8B1 and TMEM30B as essential regulators of membrane lipid asymmetry in OHCs and reveal a previously underappreciated role for lipid flippase pathways in hair cell function and survival.

Results

ATP8B1 is specifically targeted to outer hair cell stereocilia

Of the 14 P-type ATPase flippases conserved between mice and humans, 9 localize to the plasma membrane (**Shin and Takatsu, 2025**), and transcriptomic analyses identify 4 as being expressed in hair cells (**van der Mark et al., 2013**; **Liu et al., 2018**; **Kolla et al., 2020**). Recent work has implicated several phospholipid flippases, including ATP8B1, ATP8A2, and ATP11A in auditory dysfunction (**Coleman et al., 2014**; **Pater et al., 2022**; **Stapelbroek et al., 2009**). Because available antibodies lacked sufficient specificity, we generated HA knock-in (KI) mouse lines for ATP8A1, ATP8A2, ATP8B1, and ATP11A (**Figure 1B–C**). Importantly, *Atp8b1*^{HA} mice exhibited normal hearing thresholds compared to C57BL/6 J controls at P30, indicating that insertion of the HA tag did not impair auditory function (**Figure 1—figure supplement 1**). Together, these data support the use of the *Atp8b1*^{HA} knock-in allele for localization studies. Among these candidates, ATP8B1 was the only flippase specifically enriched in the hair bundle of OHCs, consistent with previous studies reporting ATP8B1-dependent hair-cell degeneration and hearing loss (**Stapelbroek et al., 2009**). Remarkably, no ATP8B1-HA immunoreactivity was detected in IHCs or their hair bundles. We performed a developmental time course of

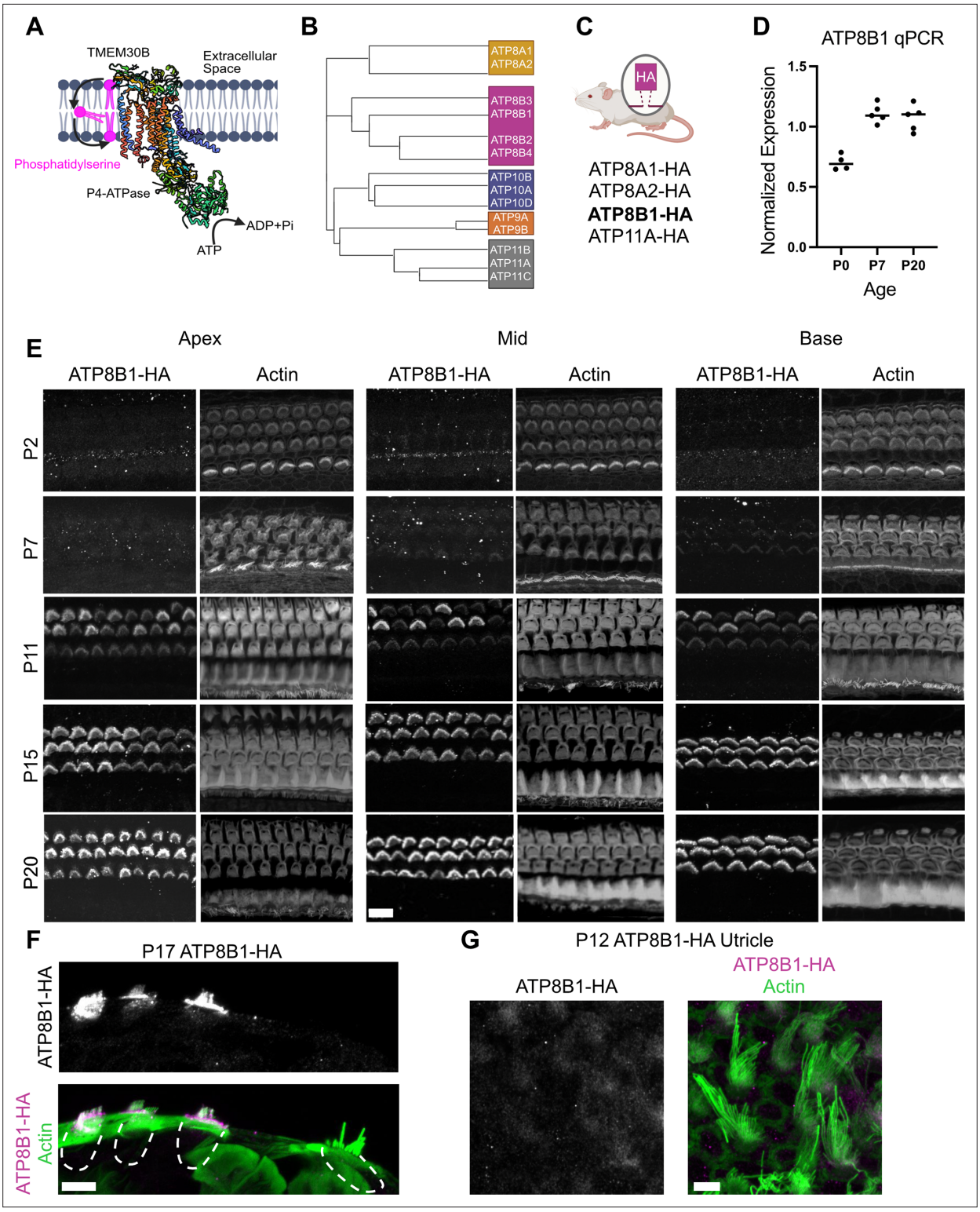


Figure 1. ATP8B1 is a P4-ATPase flippase selectively expressed in outer hair cells. (**A**) Schematic of the proposed ATP8B1–TMEM30B complex in the plasma membrane, based on the ATP8B1–TMEM30A structure (PDB 8OX4; ***Dieudonné et al., 2023***). Created with BioRender. (**B**) Cladogram of the 14 P4-ATPase family members expressed in mice. Created with BioRender. (**C**) Of the 14 P4-ATPases, 4 were detected in hair cells, and HA knock-in mouse lines were generated for each. ATP8B1-HA (bold) was the only flippase found to be expressed in outer hair cells. Created with BioRender. (**D**) qPCR analysis of *Atp8b1* expression at P0, P7, and P20. Four to five cochleae were analyzed per age group (bar represents median value). (**E**) ATP8B1-HA immunofluorescence across development and along the cochlear tonotopic axis in the organ of Corti. Organs of Corti were stained for anti-HA and

Figure 1 continued on next page

Figure 1 continued

phalloidin for F-actin. (**F**) Orthogonal view of ATP8B1-HA immunofluorescence in a P17 organ of Corti. A Compresstome section was used to facilitate imaging of the hair bundle plane. Scale bar: 5 μm. (**G**) ATP8B1-HA immunofluorescence in P12 utricle showing minimal expression. Scale bar: 10 μm.

The online version of this article includes the following figure supplement(s) for figure 1:

Figure supplement 1. *Atp8b1*^{HA} *and Tmem30b*^{HA} mice have normal hearing.

expression. Organs of Corti from *Atp8b1*^{HA} mice were imaged at key stages spanning hair-cell maturation: P2 (around the onset of MET activity), P7 (MET established but prior to hearing onset), P11 (near hearing onset), P15, and P20 (mature auditory epithelium; ***Figure 1E***). Across this timeline, ATP8B1 became progressively enriched in OHC stereocilia, coinciding with maturation of MET function and hearing onset. Protein expression patterns matched transcript levels, as qPCR analysis for *Atp8b1* demonstrated a developmental trajectory consistent with our immunofluorescence data (***Figure 1D***).

Finally, we assessed whether ATP8B1 is restricted to the stereocilia or distributed throughout the hair cell. ATP8B1-HA localized almost exclusively to OHC bundles and the apical membrane, with minimal staining in the remaining plasma membrane (***Figure 1F***). In contrast, staining of the utricle revealed only weak ATP8B1-HA signal in vestibular hair cells, markedly lower than that observed in OHCs (***Figure 1G***). Together, these data establish ATP8B1 as a tightly localized flippase that becomes strongly bundle-enriched during OHC maturation, with substantially lower expression in vestibular hair cells, and showed no detectable signal in IHCs.

We next investigated the precise subcellular localization of ATP8B1 in OHC stereocilia. OHCs oriented in profile were identified and imaged. Quantitative fluorescence intensity profiling of ATP8B1-HA and actin along both short (row 2) and tall (row 1) stereocilia revealed that ATP8B1 is present in all stereocilia rows. Notably, ATP8B1 is not uniformly distributed along the length of the stereocilia; instead, it is enriched at the stereociliary base, with signal intensity progressively decreasing toward the tips (***Figure 2A, B, C and D***).

Loss of ATP8B1 leads to early-onset hearing loss and rapid OHC degeneration

To define the role of ATP8B1 in auditory function, we generated an *Atp8b1* knockout (KO) mouse (19 bp deletion allele disrupting the translational start). Examination of the cochlea revealed a rapid and progressive loss of OHCs, beginning in the basal turn by postnatal day 17 and extending apically over the next several days (***Figure 3A and B***). By P20, only a small number of basal OHCs remained (***Figure 3B and C***). In contrast, IHCs, in which we did not detect ATP8B1, were preserved (***Figure 3D***),

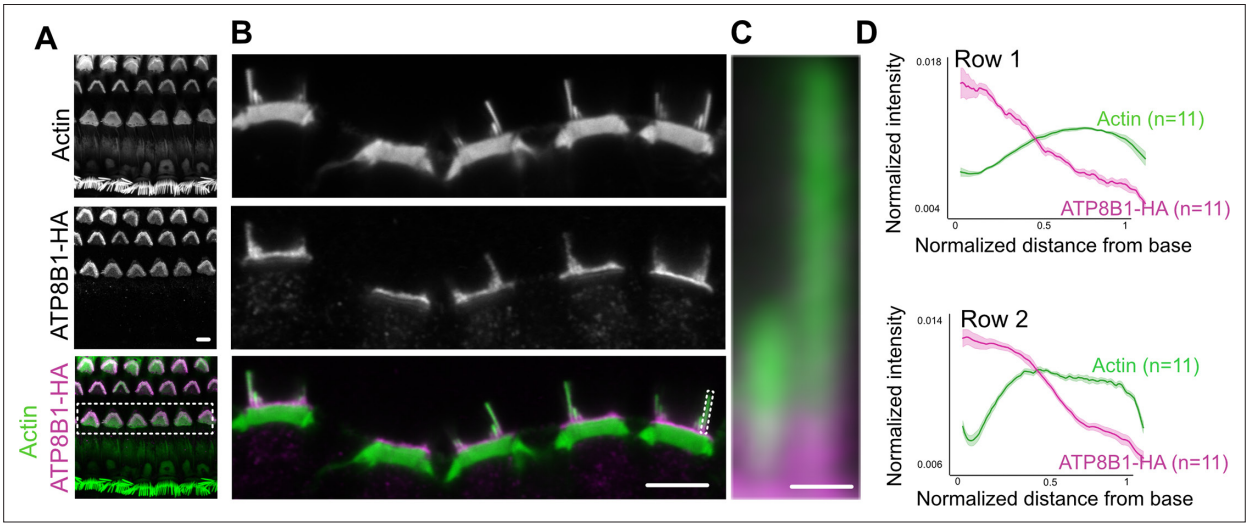


Figure 2. ATP8B1 is enriched toward the base of stereocilia. (**A**) ATP8B1-HA immunofluorescence showing OHC-specific expression. (**B,C**) ATP8B1-HA IF is enriched toward the stereocilia base and the apical hair cell membrane. (**D**) Average normalized fluorescence intensity profiles of actin and ATP8B1 along short (row 2) and long (row 1) stereocilia. Position is normalized from 0 (base) to 1 (tip), and intensities are normalized to total signal per stereocilium. Shaded regions indicate SEM. (Scale bars: 5 μm and 0.5 μm in stereocilia inset).

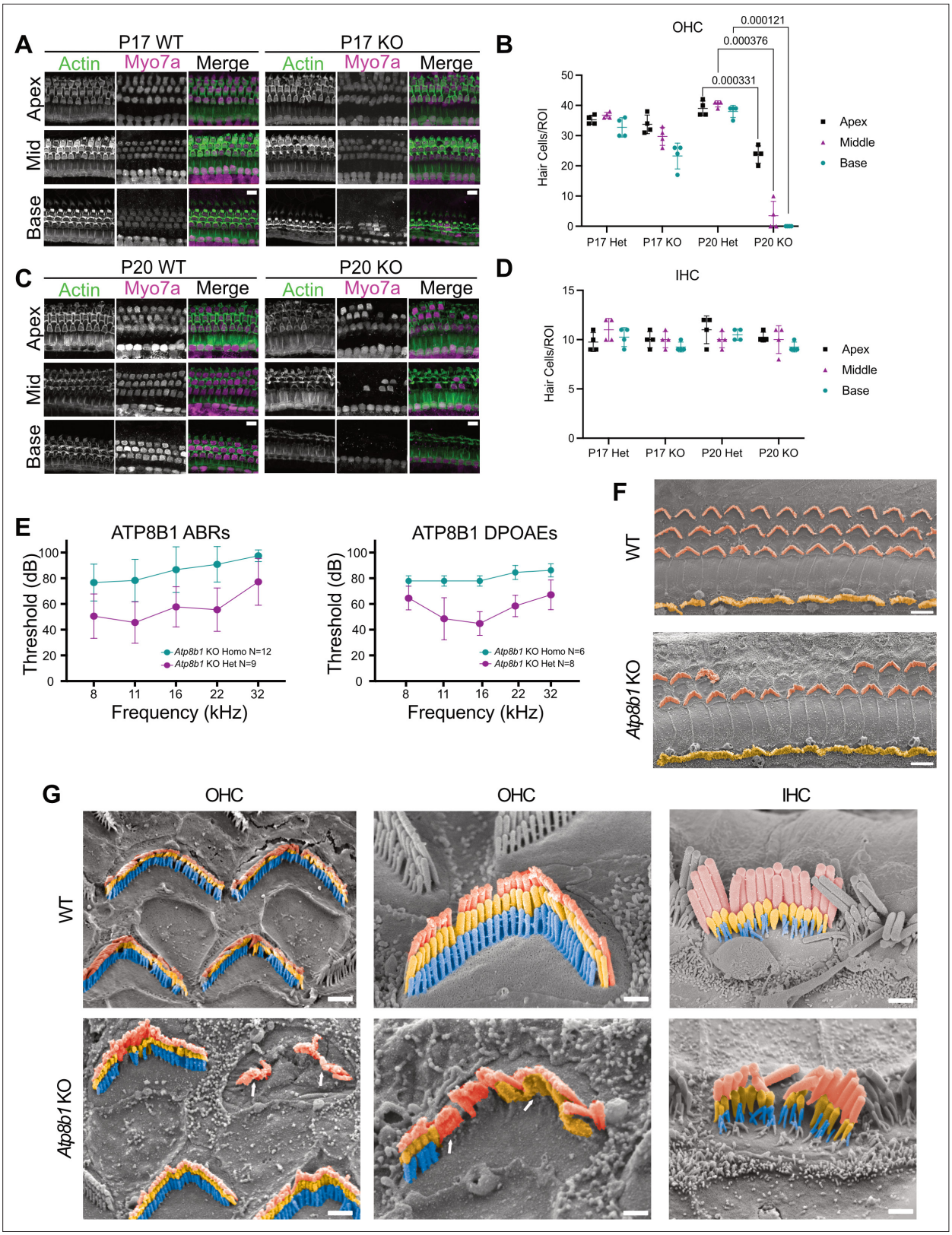


Figure 3. Loss of ATP8B1 causes progressive OHC bundle degeneration, hair cell loss, and elevated auditory thresholds. (**A,C**) Representative immunofluorescence images of WT and *Atp8b1* KO cochleae at P17 and P20 stained for MYO7A (hair cells) and phalloidin (F-actin). OHC loss is first observed in the basal turn of *Atp8b1* KO cochleae. Scale bar: 10 µm. (**B**) Quantification of OHC numbers in WT and *Atp8b1* KO cochleae at P17 and P20 across apical, middle, and basal turns (n=3–5 cochleae per group). At P20, OHC loss was significant in all tonotopic regions in KO mice compared with

Figure 3 continued on next page

Figure 3 continued

WT (Welch's t-test, p<0.001, error bars represent SD), whereas no significant differences were observed at P17. (**D**) Quantification of IHC survival in WT and *Atp8b1* KO cochleae at P17 and P20 across apical, middle, and basal turns (n=3–5 cochleae per group). No significant differences were detected between genotypes at either age (Welch's t-test, error bars represent SD). (**E**) Auditory brainstem response (ABR) thresholds at P20 are significantly elevated in *Atp8b1* KO mice compared with littermate controls (KO, N=12; WT, N=9). Distortion product otoacoustic emissions (DPOAE) thresholds at P20 are also significantly elevated (KO, N=6; WT, N=8). ABR thresholds were increased at all tested frequencies (8, 11, 16, 22, and 32 kHz; Mann–Whitney U test, p<0.001, symbol represents mean, error bars represent SD). DPOAE thresholds were elevated at all tested frequencies (8, 11, 16, 22, and 32 kHz; Mann–Whitney *U* test: $p < 0.01$ at 8 kHz; $p < 0.001$ at 11–32 kHz). Symbols represent the mean, and error bars represent SD. (**F**) Scanning electron microscopy (SEM) images of WT and *Atp8b1* KO organs of Corti at P20. OHCs are pseudo-colored orange and IHCs yellow. Scale bars: 5 µm. (**G**) High-magnification SEM images at P20 reveal stereocilia fusion and OHC loss in *Atp8b1* KO mice, features absent in WT. Arrows point out areas of stereocilia fusion and loss. IHCs remain morphologically intact. Scale bars: 1 µm (left), 0.5 µm (middle and right).

indicating a selective requirement for ATP8B1 in OHC survival. Consistent with this cellular phenotype, *Atp8b1* KO mice exhibited early-onset hearing loss. Auditory brainstem response (ABR) thresholds and distortion product otoacoustic emissions (DPOAEs) were significantly elevated across all tested frequencies at P20 compared with littermate controls, consistent with loss of OHC function (***Figure 3E***). This phenotype mirrors that previously reported for an independent *Atp8b1* point-mutation allele (***Stapelbroek et al., 2009***). Together, these findings demonstrate that ATP8B1 is essential for OHC survival and auditory function.

Following the observed hair cell loss of *Atp8b1* KO mice, we performed scanning electron microscopy (SEM) to assess hair-bundle morphology and cell integrity (***Figure 3F***). *Atp8b1* KO OHCs showed marked morphological deterioration, characterized by reduced transducing stereocilia number and occasional fusion along the edges of stereocilia rows, a known pathological feature associated with progressive hearing loss (***Figure 3G***). In contrast, IHCs did not exhibit detectable bundle abnormalities or cell loss, consistent with our immunohistochemistry results. Notably, stereocilia degeneration and fusion in the KO mice occurred prior to overt hair cell loss, indicating that disruption of bundle architecture is an early consequence of ATP8B1 deficiency.

TMEM30B expression and localization mirrors that of ATP8B1

The targeting and function of P-type ATPase flippases require association with β-subunits TMEM30A or TMEM30B. To determine which partners operate with ATP8B1 in OHCs, we created HA-tagged KI mice for both proteins. TMEM30B, but not TMEM30A (data not shown), was targeted to hair cell stereocilia. *Tmem30b*^{HA} mice exhibited normal hearing thresholds compared with C57BL/6 J controls at P30, indicating that insertion of the HA tag did not disrupt auditory function (***Figure 1—figure supplement 1***). Organs of Corti from *Tmem30b*^{HA} mice were imaged at P2, P7, P11, P17, and P20 (***Figure 4A***). Across this series, TMEM30B-HA showed a progressive enrichment in stereocilia, paralleling the maturation of the MET apparatus and the onset of hearing, similar to ATP8B1. We next studied the subcellular distribution of TMEM30B. While ATP8B1-HA was almost exclusively confined to OHC bundles (***Figures 1 and 2***), TMEM30B-HA was enriched in the stereocilia compartment, but also weakly in the cell body (***Figure 4B***). Like ATP8B1-HA, TMEM30B-HA showed modest labeling of utricular hair bundles at P17 (***Figure 4C***) and was excluded from IHC bundles. Together, these findings identify ATP8B1 and TMEM30B as a tightly co-localized flippase complex that becomes progressively OHC bundle-specific during auditory maturation.

TMEM30B is required for hearing and OHC maintenance

Next, we generated *Tmem30b* KO mice harboring a 54 bp deletion disrupting the translational start. Similar to *Atp8b1* KO mice, *Tmem30b* KO mice exhibited rapid OHC degeneration, beginning in the basal turn at P17 and advancing apically over the following days. By P20, only a small number of basal OHCs remained (***Figure 5A and B***). In contrast, IHCs were preserved, closely mirroring the *Atp8b1* KO phenotype and indicating that loss of TMEM30B selectively compromises OHC survival (***Figure 5C and D***). Consistent with this cellular phenotype, *Tmem30b* KO mice exhibited early-onset hearing loss. ABR thresholds and DPOAEs were significantly elevated across all tested frequencies at P30 compared with littermate controls, consistent with loss of OHC function (***Figure 5E***). Together, these findings confirm TMEM30B as a deafness gene, in agreement with an auditory phenotype previously reported by the IMPC (International Mouse Phenotyping Consortium; ***Bowl et al., 2017***).

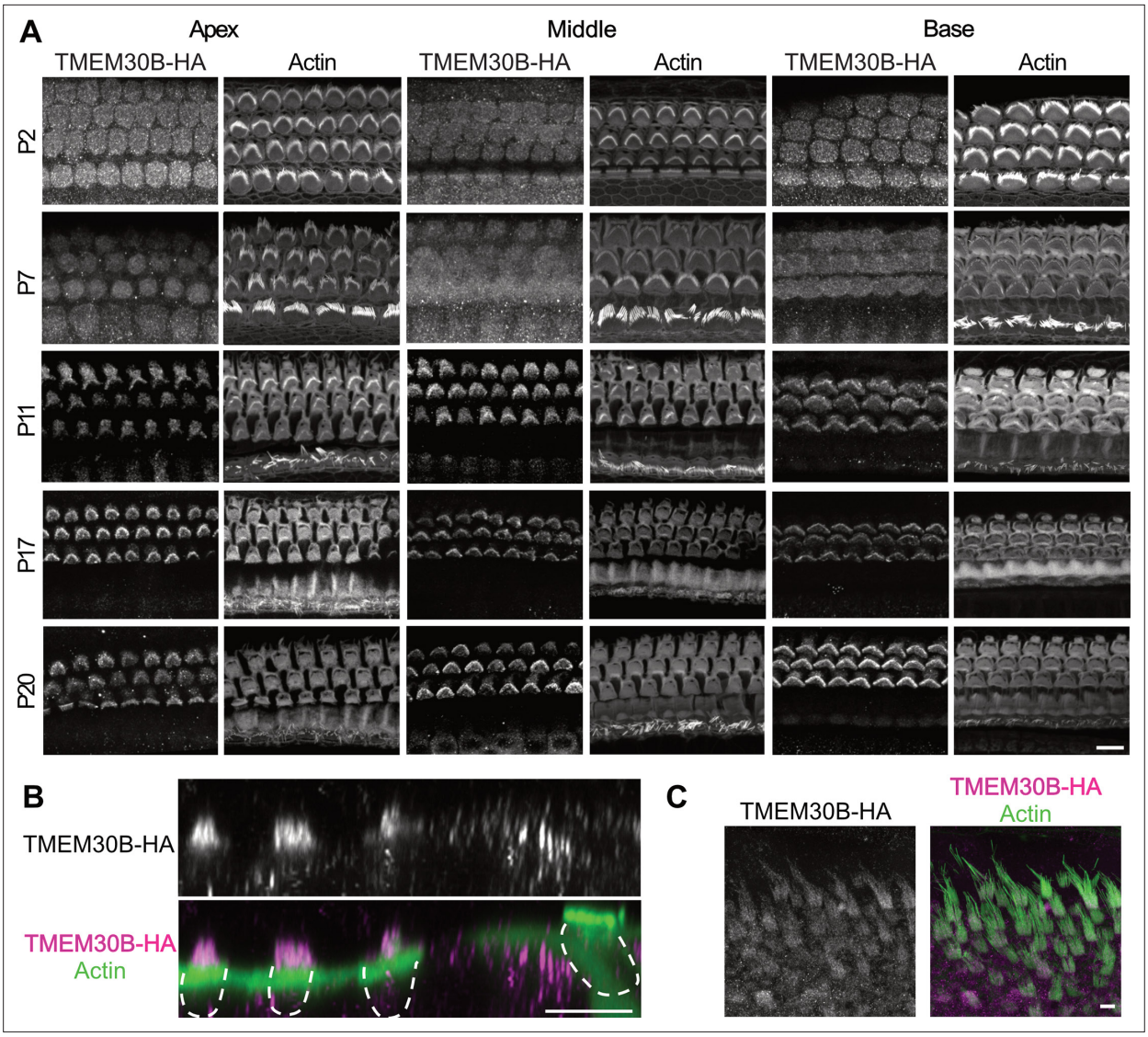


Figure 4. The P4-ATPase chaperone TMEM30B is enriched in OHC bundles. (**A**) Immunofluorescence images of TMEM30B-HA across development and along the cochlear tonotopic axis in the organ of Corti. Organ of Corti were stained for anti-HA and phalloidin for F-actin. Scale bar: 10 μm. (**B**) Orthogonal view of TMEM30B-HA immunofluorescence of a P17 organ of Corti. Scale bar: 10 μm. (**C**) Immunofluorescence images of a P17 TMEM30B-HA utricle showing moderate expression in utricular hair cells. Scale bar: 10 μm.

We next performed SEM analysis to assess the morphological defects in *Tmem30b* KO OHC hair bundles (***Figure 5F***). Prior to overt cell loss, *Tmem30b* KO OHCs exhibited fractured and disorganized hair bundles. We did not observe the same hair bundle fusion that occurred in the *Atp8b1* KO OHCs, possibly pointing to a difference in cell deterioration between the two mouse lines (***Figure 5G***). IHCs displayed no detectable morphological abnormalities. Overall, the degenerative phenotype in *Tmem30b* KO mice largely parallels that of *Atp8b1* KO mice, supporting a shared requirement for the ATP8B1-TMEM30B flippase complex in maintaining OHC integrity.

To determine how the loss of TMEM30B affects the localization of ATP8B1-HA, we examined ATP8B1-HA localization on the *Tmem30b* KO mouse background. In control mice, ATP8B1-HA is enriched in stereocilia and not found below the hair bundle and the apical membrane. In contrast, in the absence of TMEM30B, ATP8B1-HA showed markedly increased somatic staining with reduced confinement to the hair bundle, indicating protein mislocalization (***Figure 5H***). These findings demonstrate that TMEM30B is necessary for correct targeting of ATP8B1, providing a mechanistic explanation for the closely overlapping phenotypes observed in the two KO models.

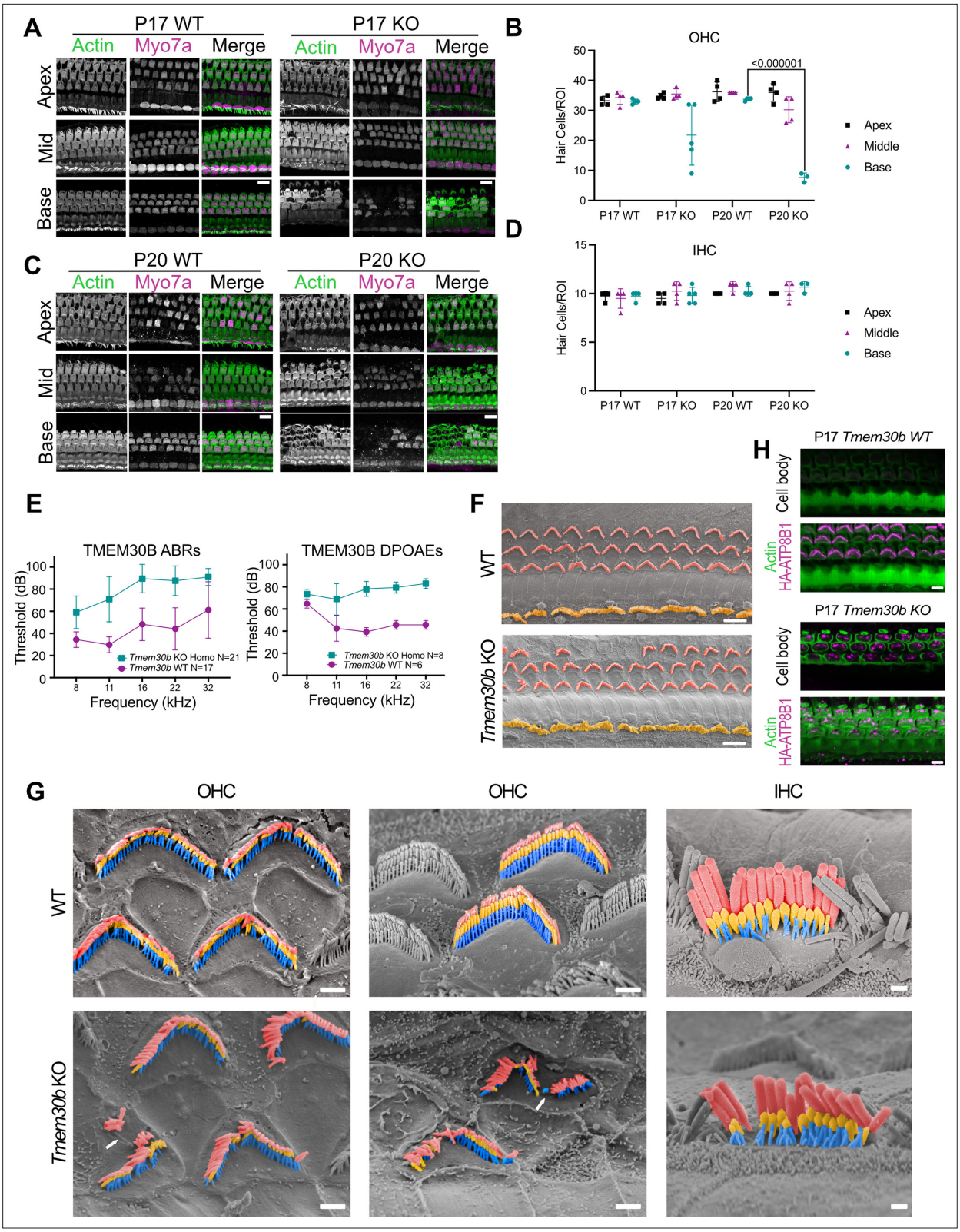


Figure 5. Loss of TMEM30B causes progressive OHC degeneration, hair cell loss, and elevated auditory thresholds. (**A, C**) Representative immunofluorescence images of WT and *Tmem30b* KO cochleae at P17 and P20, stained for MYO7A (hair cells) and phalloidin (F-actin). OHC loss is first detected in the basal turn of *Tmem30b* KO cochleae at P17, and pronounced OHC loss in the basal turn of KO cochleae at P20. Scale bar: 10 μm. (**B**) Quantification of OHC numbers in WT and *Tmem30b* KO cochleae at P17 and P20 across apical, middle, and basal turns (n=3–5 cochleae per group). At

Figure 5 continued on next page

Figure 5 continued

P20, OHC loss was significant in the basal region of KO mice compared with WT (Welch's *t*-test, p<0.001, error bars represent SD), whereas no significant differences were observed at P17. (**D**) Quantification of IHC numbers in WT and *Tmem30b* KO cochleae at P17 and P20 across apical, middle, and basal turns (n=3–5 cochleae per group). No significant differences were detected between genotypes at either age (Welch's *t*-test, error bars represent SD). (**E**) Auditory brainstem response (ABR) thresholds at P30 are significantly elevated in *Tmem30b* KO mice compared with littermate controls (KO, N=21; WT, N=17). Distortion product otoacoustic emissions (DPOAE) thresholds at P30 are also significantly elevated (KO, N=8; WT, N=6). ABR and DPOAE thresholds were increased at all tested frequencies (8, 11, 16, 22, and 32 kHz; Mann–Whitney U test, p<0.001, symbol represents mean, error bars represent SD). (**F**) Scanning electron microscopy (SEM) images of WT and *Tmem30b* KO organs of Corti at P20. OHCs are pseudo-colored orange and IHCs yellow. Scale bars: 5 µm. (**G**) High-magnification SEM images at P20 reveal stereocilia misorientation and OHC loss in *Tmem30b* KO mice, features absent in WT. Arrows point out areas of stereocilia misorientation. IHCs remain morphologically intact. Scale bars: 1 µm (left), 0.5 µm (middle and right). (**H**) Immunofluorescence images of organs of Corti from *Atp8b1*^{HA} KI/*Tmem30b* KO mice at P17 showing aberrant localization of ATP8B1-HA to the hair cell soma in the absence of TMEM30B (magenta). Scale bars: 5 µm.

ATP8B1 and TMEM30B deficiency causes aberrant PS exposure in OHC bundles

ATP8B1 deficiency is predicted to impair PS internalization from the outer plasma membrane leaflet (***Klomp et al., 2004***). Persistent PS exposure could disrupt MET function and/or initiate downstream pathways that contribute to hair-cell degeneration as observed in both KO mouse models. We therefore examined whether *Atp8b1* and *Tmem30b* KO OHCs exhibit abnormal PS exposure. We performed Annexin V (AnV) labeling on apical turns of P15 organs of Corti (***Zhang et al., 1997***), a developmental timepoint that precedes overt hair cell loss in these mutants (***Koopman et al., 1994***; ***Figure 6A and C***). AnV labeling was restricted to the stereocilia bundle and apical membrane and not detected along the lateral membrane or within the cell body. Both *Atp8b1* KO and *Tmem30b* KO mice exhibited significantly elevated AnV fluorescence compared with wild-type controls (***Figure 6B and D***). We occasionally observed weak AnV labeling also in IHCs, at the apical membrane (often appearing to be enriched at cell junctions) and the hair bundle (***Figure 6A and C***). Together, these findings indicate that loss of ATP8B1-TMEM30B flippase activity leads to aberrant PS exposure predominantly in OHC stereocilia, preceding and likely contributing to hair cell degeneration in both KO models.

Discussion

In this study, we identify P4-ATPase ATP8B1 and its accessory subunit TMEM30B as essential regulators of OHC survival and auditory function. Our findings establish a direct mechanistic link between OHC stereocilia membrane lipid asymmetry and hearing by demonstrating that disruption of a stereocilia-localized flippase complex leads to aberrant PS exposure, early hair-bundle pathology, progressive OHC degeneration, and rapid hearing loss. Together, these data reveal a previously underappreciated requirement for active lipid homeostasis in OHCs and provide cellular and mechanistic validation of TMEM30B as a novel deafness gene.

A flippase complex is selectively enriched in OHC stereocilia

A central finding of this work is the highly selective localization of ATP8B1 and TMEM30B to OHC stereocilia. Among the P4-ATPases expressed in hair cells, ATP8B1 uniquely localizes to the hair bundle, was not detectably enriched in IHCs, and becomes progressively enriched in hair bundles during postnatal maturation, coinciding with the onset and maturation of hair cell MET. This specificity likely serves to accommodate the uniquely high mechanical and metabolic demands placed on OHC stereocilia. ATP8B1 is strongly enriched within stereocilia membranes, with minimal localization in the plasma membrane below the epithelial barrier level. Loss of TMEM30B results in mislocalization of ATP8B1, demonstrating that this β-subunit is required not only for flippase activity but also for proper targeting and retention of ATP8B1 in the stereocilia membrane.

Lipid asymmetry as a potential structural and functional determinant of MET

Recent cryo-EM studies, together with the discovery that TMC1 and TMC2 possess intrinsic lipid-scrambling activity, have prompted a re-evaluation of MET in which membrane lipids and their asymmetric distribution are re-considered as active determinants of channel function rather than passive

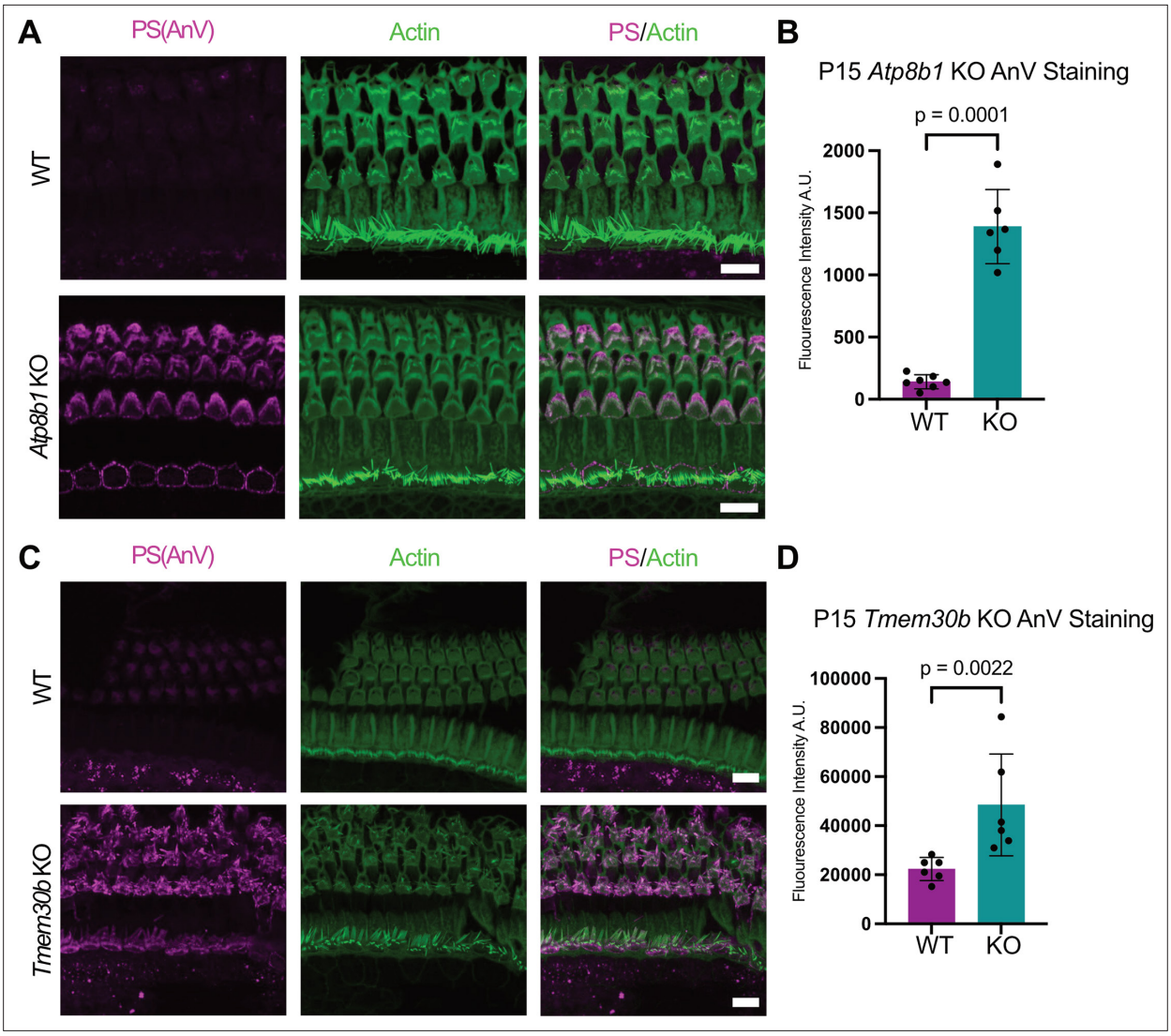


Figure 6. Loss of plasma membrane asymmetry precedes hair cell loss in *Atp8b1* and *Tmem30b* knockout mice. (**A**) Representative confocal images of WT and *Atp8b1* KO cochleae at P15 stained with Annexin V to label externalized phosphatidylserine (PS) and phalloidin to visualize F-actin. Increased Annexin V labeling is observed in *Atp8b1* KO hair cells prior to overt cell loss. Scale bar: 10 µm. (**B**) Quantification of Annexin V fluorescence intensity in WT and *Atp8b1* KO cochleae (n=5–7 cochleae per group). *Atp8b1* KO hair cells show significantly increased PS externalization compared with WT (Welch's *t*-test, p=0.0001, error bars represent SD). (**C**) Representative confocal images of WT and *Tmem30b* KO cochleae at P15 stained with Annexin V and phalloidin. Increased Annexin V labeling is similarly observed in *Tmem30b* KO hair cells. In *Atp8b1* and *Tmem30b* KO organs of Corti, weak AnV labeling was occasionally observed also in IHCs, at the apical cell junctions and the hair bundle. Scale bar: 10 µm. (**D**) Quantification of Annexin V fluorescence intensity in WT and *Tmem30b* KO cochleae (n=5–7 cochleae per group), demonstrating significantly elevated PS externalization in KO hair cells (Welch's *t*-test, p<0.01, error bars represent SD).

structural components (***Ballesteros and Swartz, 2022***; ***Jeong et al., 2022***; ***Clark et al., 2024***; ***Peineau et al., 2025***). Loss of membrane lipid asymmetry, particularly the redistribution of lipids with bulky and charged headgroups such as PS, is known to have profound biophysical consequences for cellular membranes (***Kakuda et al., 2022***; ***Li et al., 2024***; ***Wang et al., 2025***), and the stereocilia membrane will not be an exception. Redistribution of PS to the outer leaflet alters bilayer thickness (***Wang et al., 2025***), curvature stress, and membrane viscosity (***Caputo et al., 2025***), parameters that are particularly critical in stereocilia (***George et al., 2020***; ***Sam George et al., 2023***; ***George and Ricci, 2026***), where MET channel gating is exquisitely sensitive to membrane mechanics.

Building on this framework, a recent model proposed by George and Ricci suggests that TMC1/2 scramblase activity, by lowering membrane viscosity, reduces the energetic cost of channel gating, which may improve both the speed and sensitivity of the MET response (***George and Ricci, 2026***).

If lipid scrambling is an integral feature of MET, however, a compensatory mechanism must exist to prevent unchecked collapse of membrane asymmetry. It is tempting to speculate that the ATP8B1-TMEM30B flippase complex fulfills this role by continuously restoring lipid asymmetry and maintaining OHC membranes within a 'Goldilocks zone' of viscosity optimal for OHC MET.

This model is supported by the spatial distribution of ATP8B1, which is most abundant at the base of stereocilia and within the apical OHC membrane, with decreasing levels toward the stereocilia tips where MET occurs. Such a gradient suggests that TMC1-mediated lipid scrambling predominates at the site of MET, while ATP8B1-TMEM30B activity at the bundle base and apical membrane prevents widespread PS exposure, which could be interpreted as an 'eat-me' signal and trigger pathological and phagocytic responses by surrounding supporting cells. Consistent with this model, elevated PS exposure in both *Atp8b1* and *Tmem30b* KO hair cells precedes overt structural degeneration, indicating that continuous flippase activity is required to preserve stereociliary membrane composition and stability.

Selective requirement for stereocilia flippase activity in OHCs versus IHCs

A striking aspect of our findings is that in the cochlea, ATP8B1 is selectively expressed in OHC stereocilia and was not detected in IHCs under the conditions examined. One possible explanation is that IHC stereocilia express another flippase. This seems unlikely as we systematically assessed all P4-ATPases expressed in hair cells and did not find evidence for an alternative stereocilia-enriched P4-ATPase in IHC bundles. Instead, we think it likely that IHCs, at least in the stereocilia, lack flippase activity altogether. It is possible that IHCs maintain lipid asymmetry using a different strategy, for example, by relying on a distinct set of lipid transporters localized outside the bundle, possibly sufficient given the lower MET resting open probability in IHCs (***Johnson et al., 2011***; ***Peng et al., 2013***; ***Corns et al., 2014***), resulting in lower basal scrambling pressure. It is also possible that beyond P4-ATPase flippases, complementary regulation could also arise from other enzymes controlling lipid abundance (synthesis and degradation) and compartmentalization (***Blom et al., 2011***).

Early bundle pathology precedes hair-cell loss

Annexin V-mediated detection of PS and structural analyses reveal that PS externalization and hair-bundle degeneration precede hair-cell death in both KO models. Notably, IHCs remain morphologically and functionally intact, consistent with their lack of ATP8B1 and TMEM30B expression. This selective vulnerability underscores the unique lipid homeostasis requirements of OHC stereocilia, likely reflecting an adaptation to their higher MET activity and mechanical load. A recent study reported Annexin V labeling of hair bundles beginning around P7 in wild-type mouse OHCs, suggesting PS exposure on the outer leaflet during normal development (***George and Ricci, 2026***). This observation contrasts with our findings, in which robust and consistent Annexin V labeling was observed only in *Atp8b1* and *Tmem30b* KO hair cells. We note, however, that we occasionally detected low-level Annexin V signal in control samples, even in IHCs (as shown in ***Figure 6***). Given the sensitivity of the live Annexin V labeling procedure to rapid deterioration of cochlear hair cells, particularly OHCs after ototoxic insult (***Shi et al., 2007***; ***Goodyear et al., 2008***), this signal was initially interpreted as background or false-positive staining. Nonetheless, an alternative explanation is that OHC stereocilia possess higher PS exposure under normal physiological conditions, an expected phenomenon if TMC1/2-mediated MET causes phospholipid scrambling. Such low-level exposure of PS may fall near the detection threshold of Annexin V staining, especially if quickly reversed by flippase activity, and thus be difficult to resolve reproducibly. Further work will be required to determine whether regulated, developmentally controlled phospholipid exposure occurs in normal hair bundles and how it is balanced by flippase activity.

Why do ATP8B1/TMEM30B-deficient OHCs die?

One notable feature of *Atp8b1* and *Tmem30b* KO phenotypes is their fast-progressing, base-to-apex pattern of OHC loss, reminiscent of several models in which MET is disrupted (e.g. TMC1/2 or CIB2 loss and related MET-deficient conditions; ***Kawashima et al., 2011***; ***Riazuddin et al., 2012***; ***Zhao et al., 2014***; ***Pan et al., 2018***; ***Beurg et al., 2025***). Loss of lipid asymmetry could directly compromise MET by altering bundle membrane mechanics and/or the availability of lipids on the inner leaflet

that are required for normal MET. In this model, OHC degeneration would arise downstream of impaired MET signaling. At the same time, the OHC-specific degeneration observed in *Atp8b1* and *Tmem30b* KO mice also parallels, both in kinetics and cellular selectivity, the phenotype reported in mice with impaired stereocilia calcium extrusion via PMCA2 (**Street et al., 1998**; **Kozel et al., 1998**; **Beurg et al., 2025**). Loss of lipid asymmetry and/or altered phosphoinositide organization could reduce PMCA2 efficiency, compromising calcium clearance from stereocilia and promoting cytotoxic calcium accumulation. Consistent with this general possibility, PMCA activity is known to depend on membrane lipid composition. Specifically, PS on the inner leaflet was shown to be required for optimal PMCA activity (**Zhang et al., 2009**).

Limitations of this study

A limitation of the present study is that loss of lipid asymmetry in OHC stereocilia was assessed primarily through PS externalization, as detected by Annexin V binding. Annexin V is a widely used indicator of disrupted membrane asymmetry, and the absence of PS exposure in WT mice, together with its robust appearance in ATP8B1- and TMEM30B-deficient OHCs, supports a role for ATP8B1 in maintaining membrane lipid organization. However, this approach specifically reports PS exposure and does not directly inform on the asymmetric distribution of other lipid species. ATP8B1 has been reported to transport PS in several experimental contexts, and our data are therefore fully consistent with the possibility that PS is a direct substrate of ATP8B1 in OHC stereocilia membranes. At the same time, independent evidence from cell-based, biochemical, and structural studies indicates that ATP8B1 can also transport PC and phosphoinositides, with recent work demonstrating ATP8B1-mediated flipping of $PI(4,5)P_2$ (**Takatsu et al., 2014**; **Gómez-Mellado et al., 2022**; **Dieudonné et al., 2022**; **Bhandari et al., 2025**). Consequently, the PS externalization observed in *Atp8b1* and *Tmem30b* KO mice may reflect loss of asymmetry of PS itself, of other ATP8B1 substrates, or of multiple lipid species simultaneously. Because robust in situ reporters for leaflet-specific PC or phosphoinositide distribution are currently limited, our study cannot directly distinguish among these possibilities. Thus, while PS exposure provides a clear and biologically meaningful readout of altered lipid asymmetry, it should not be interpreted as indicating that ATP8B1 function in stereocilia is exclusively or primarily PS-centric. Instead, our findings support a broader role for ATP8B1 in maintaining the asymmetric organization of stereocilia membranes, with PS externalization serving as a sensitive marker of this process.

Future studies employing lipid-specific biosensors, reconstitution-based approaches, or advanced lipidomic strategies may be important for defining the full spectrum of ATP8B1 substrates in stereocilia and for determining how perturbations in distinct lipid species contribute to OHC structure and function.

TMEM30B as a deafness gene and therapeutic implications

While ATP8B1 has been previously implicated in hearing loss, evidence was limited and mechanistic insight lacking (**Stapelbroek et al., 2009**). Our data provide strong validation of ATP8B1's role in hearing and identify TMEM30B as an essential partner whose loss phenocopies ATP8B1 deficiency at molecular, cellular, and functional levels. These findings align with a previous large-scale mouse mutagenesis screen reporting hearing loss in *Tmem30b* KO mice (**Bowl et al., 2017**). Importantly, ATP8B1 and TMEM30B have attractive therapeutic features. Their expression begins postnatally and peaks after hearing onset in mice, and hair-cell loss in KO mice occurs after ~P16, providing a potential window for intervention. Furthermore, TMEM30B is a single-exon gene of modest size (~3.5 kb including UTRs), making it well suited for AAV-mediated gene delivery and faithful recapitulation of endogenous expression. While our manuscript was under review, **Chang et al., 2026** independently showed that loss of *Tmem30b* causes hearing loss in mice and reported largely concordant findings on the expression and subcellular localization of TMEM30B and ATP8B1, their interaction, and the auditory phenotypes associated with their loss. Chang et al. also showed that AAV-mediated delivery of *Tmem30b* partially alleviated stereocilia defects in both *Tmem30b*- and *Atp8b1*-deficient mice, supporting the therapeutic potential of this approach.

Conclusions and future directions

In summary, this study establishes ATP8B1 and TMEM30B as important regulators of membrane lipid asymmetry in OHC stereocilia and hair-cell survival, and points to a potentially essential role for lipid

flipping in hair cell MET. Future studies will be required to quantify, using cellular electrophysiology, how lipid asymmetry influences MET channel gating and sensitivity, and to determine which additional lipid species are regulated by ATP8B1 in stereocilia.

Materials and methods

Key resources table

Reagent type (species) or resource	Designation	Source or reference	Identifiers	Additional information
Genetic Reagent (*Mus musculus*)	C57BL/6J	The Jackson Laboratory	RRID:IMSR_JAX:000664	
Genetic Reagent (*Mus musculus*)	*Atp8b1*^{HA} KI	This paper	—	See 'Generation of experimental mice'/'Resource availability'
Genetic Reagent (*Mus musculus*)	*Tmem30b*^{HA} KI	This paper	—	See 'Generation of experimental mice'/'Resource availability'
Genetic Reagent (*Mus musculus*)	*Atp8b1* KO	This paper	—	See 'Generation of experimental mice'/'Resource availability'
Genetic Reagent (*Mus musculus*)	*Tmem30b* KO	This paper	—	See 'Generation of experimental mice'/'Resource availability'
Genetic Reagent (*Mus musculus*)	*Atp8b1*^{HA} KI/*Tmem30b* KO	This paper	—	See 'Generation of experimental mice'/'Resource availability'
Antibody	Rabbit monoclonal anti-HA	Cell Signaling Technology	C29F4, RRID:AB_1549585	1:200
Antibody	Rabbit polyclonal anti-MYO7A	Proteus Biosciences Inc, Ramona, CA	25–6790, RRID:AB_10015251	1:200
Antibody	Alexa Fluor 555-donkey-anti-rabbit conjugated secondary antibody	Thermo Fisher Scientific	Cat # A-31572, RRID:AB_162543	1:200
Antibody	Alexa Fluor 647-donkey-anti-rabbit conjugated secondary antibody	Thermo Fisher Scientific	Cat # A-31573, RRID:AB_2536183	1:200
Chemical compound/reagent	Phalloidin Alexa Fluor 488	Thermo Fisher Scientific	Cat # A12379	1:200
Commercial assay/kit	Alexa Fluor 488-conjugated Annexin V	Thermo Fisher Scientific	Cat # A13201	1:25
Sequence-based reagent	*Atp8b1*_F	This paper	PCR primers	AGGGGTCTTCTGACAGGATG
Sequence-based reagent	*Atp8b1*_R	This paper	PCR primers	TCTGTTCTGGTTCAACCGTGG
Sequence-based reagent	*Tmem30b*_F	This paper	PCR primers	CGCTGATCCTGGGTTGAGAG
Sequence-based reagent	*Tmem30b*_R	This paper	PCR primers	TGCCGTTGGAGGAGTAGAAG
Sequence-based reagent	*Gapdh*_F	This paper	qPCR primers	AACGACCCCTTCATTGAC
Sequence-based reagent	*Gapdh*_R	This paper	qPCR primers	TCCACGACATACTCAGCAC
Sequence-based reagent	*Atp8b1*_F	This paper	qPCR primers	ACGGCCGGTGGTCTTACATA
Sequence-based reagent	*Atp8b1*_R	This paper	qPCR primers	GCTTGTCACTCACGTCCTGAT
Chemical compound	Paraformaldehyde	Electron Microscopy Sciences	—	Fixative
Chemical compound	Glutaraldehyde	Electron Microscopy Sciences	—	Fixative
Chemical compound	EDTA	Bioland Scientific LLC	0.5 M, pH 8.0	Calcium chelator
Other	ProLong Gold Antifade Mountant	Thermo Fisher Scientific	Cat # P36930	Additional information: See "Immunofluorescence"

Continued on next page

Continued

Reagent type (species) or resource	Designation	Source or reference	Identifiers	Additional information
Other	TRIzol	Thermo Fisher Scientific	Cat # 15596026	Additional information: See 'Quantitative PCR'
Commercial assay, kit	SuperScript IV Reverse Transcription System	Thermo Fisher Scientific	Cat # 18090010	Additional information: See 'Quantitative PCR'
Commercial assay, kit	iTaq Universal SYBR Green Supermix	Bio-Rad	1725121	Additional information: See 'Quantitative PCR'
Other	CFX Opus 384 Real-Time PCR System	Bio-Rad	12011319	Additional information: See 'Quantitative PCR'
Software/algorithm	CRISPOR	***Haeussler et al., 2016***	https://crispor.gi.ucsc.edu/crispor.py; RRID:SCR_015935	See 'Generation of experimental mice'
Software	ImageJ	NIH	RRID:SCR_003070	Image analysis software
Software	GraphPad Prism	GraphPad Software	RRID:SCR_002798	Statistical analysis software
Other	Stellaris 5	Leica Microsystems	RRID:SCR_024663	Additional information: See "Immunofluorescence"
Other	Stellaris 8	Leica Microsystems	RRID:SCR_024664	Additional information: See "Annexin V staining"
Other	JSM-IT710HR InTouchScope	JEOL	RRID:SCR_018736	Scanning Electron Microscope, University of Virginia Advanced Microscopy Facility
Other	ABR recording equipment	Tucker-Davis Technologies	RRID:SCR_014820	Additional information: See "Hearing tests in mice"
Other	Subdermal needle electrodes	Grass Technologies	FE-7	Additional information: See "Hearing tests in mice"
Other	SmartOAE v5.20	Intelligent Hearing Systems	RRID:SCR_007196	Additional information: See "Hearing tests in mice"
Other	Sound isolating cubicle	Med-Associates	ENV-022MD-WF	Additional information: See "Hearing tests in mice"
Other	Deltaphase Isothermal Heating Pad	Braintree Scientific	—	Additional information: See "Hearing tests in mice"
Other	Compresstome	Precisionary Instruments	RRID:SCR_024623	Additional information: See "Immunofluorescence"

Animal care and handling

All murine experiments conducted for this study adhered to the guidelines established by the University of Virginia Institutional Animal Care and Use Committee (IACUC) and the NIH. Animal protocols were reviewed and approved by the University of Virginia IACUC. Mice were housed in an AAALAC-accredited vivarium located in the basement of our research building. Animals were maintained on a 12 hr light/dark cycle, with cage changes performed every five days. Mice had ad libitum access to standard rodent chow and water provided through lixit systems. Control mice were C57BL/6 J mice obtained from Jackson Laboratory. Experimental mice ranged from postnatal day 0 (P0) to P5 and were euthanized via rapid decapitation. Mice aged P6 and older were euthanized using CO_2 asphyxiation, followed by cervical dislocation as a secondary method to ensure humane euthanasia.

Generation of experimental mice

Genetically modified mouse models used in this study were generated using CRISPR/Cas9-mediated genome editing to create knockout or knock-in alleles of ATP8B1 and TMEM30B.

CRISPR/Cas9 target sequences were designed using the online tool CRISPOR (http://crispor.tefor.net/crispor.py) to generate KI and KO alleles for *Atp8b1* and *Tmem30b* (***Haeussler et al., 2016***). The selected guide RNA target sequences were **AAGCACAGAAAGAGACT** for *Atp8b1* and **CGCCGTGG CGCTCCAGGTCA** for *Tmem30b*.

For *Atp8b1*, the genomic sequence surrounding the target site and illustrating the KO modification is shown below:

TCAGCCCAACACAGGAAAGTCACGACTCACTCCTGTTTCCTCCTTTTCTCTCCAGGTAGT
TCCAATTTGCCAGCAGA**AT**GAGCACAGAAAGAGACTCGGAAACAACATTTGATGAGGA
GTCTCAGCCCAACGATGAAGTGGTCCCCTACAGTGATGATGA

The HA epitope-coding sequence (TACCCATACGATGTTCCAGATTACGCT) was inserted immediately downstream of the start codon (ATG, bold). The KO allele was generated by deletion of 19 nucleotides (underlined).

For *Tmem30b*, the following CRISPR target sequence was identified: **CGCCGTGGCGCTCCAG GTCA**. The genomic sequence surrounding the target site and illustrating the KO modification is shown below:

GCGAGCGGAGGCGGGAGGCTCGCCGCTGATCCTGGGTTGAGAGTCGGCGGCCGCA
GGCCCCGGCTGAGATCCCCGCCATGACCTGGAGCGCCACGGCGCGGGGCGCGCACCAG
CCCGACAACACCGCCTTCACTCAGCAGCGCCTCCCCGCCTGGCAGCC

As for ATP8B1, the HA epitope-coding sequence was inserted immediately downstream of the start codon (ATG, bold). The KO allele was generated by deletion of 54 nucleotides (underlined).

Genotyping

Genotyping of *Atp8b1* alleles yielded PCR products of 239 bp (wt), 266 bp (HA KI), and 220 bp (KO). Primers used were:

Forward: AGGGGTCTTCTGACAGGATG
Reverse: TCTGTTCTGGTTCAACCGTGG

Genotyping of *Tmem30b* alleles yielded PCR products of 232 bp (wt), 259 bp (HA KI), and 178 bp (KO). Primers used were:

Forward: CGCTGATCCTGGGTTGAGAG
Reverse: TGCCGTTGGAGGAGTAGAAG

Mouse colony maintenance

Atp8b1 KO mice were maintained as heterozygous breeders. All other lines (*Atp8b1*^{HA} KI, *Tmem30b* KO, *Tmem30b*^{HA} KI, *Atp8b1*^{HA} KI/*Tmem30b* KO) were maintained as homozygous breeding colonies.

Immunofluorescence

Mice were sacrificed via decapitation (for P5 and younger) or CO2 asphyxiation followed by cervical dislocation (for P6 and older). Cochleae were carefully dissected and placed into a dish containing phosphate-buffered saline (PBS; GIBCO, Thermo Fisher Scientific). Under a dissecting microscope, the ossicles were removed, and the cochleae were transferred to a well containing 4% paraformaldehyde (PFA; Electron Microscopy Sciences). The cochleae were flushed through the oval and round windows using a transfer pipette to ensure proper fixation and incubated in the fixative for 20 min at room temperature. After fixation, the cochleae were washed three times for five minutes each in PBS. For P7 and younger mice, cochleae were immediately dissected. For P8 and older mice, cochleae were decalcified in 0.5 M ethylenediaminetetraacetic acid (EDTA; Bioland Scientific LLC), pH 8.0, for up to 2 weeks, depending on bone density. Organs of Corti were either dissected as whole mounts under a stereomicroscope using forceps and micro-dissection scissors or sectioned into 50 µm slices using a Compresstome (Precisionary Instruments, Ashland, MA). Dissected or sliced organs of Corti were transferred to blocking buffer and incubated for 2 hr at room temperature. The blocking buffer consisted of PBS supplemented with 1% bovine serum albumin (BSA), 3% normal donkey serum, and 0.2% saponin. Following blocking, tissues were incubated overnight at 4 °C with primary antibodies diluted in the same blocking buffer. The

following primary antibody was used: rabbit anti-HA (C29F4, Cell Signaling Technology, Danvers, MA). The next day, tissues were washed three times for 5 min each in PBS, then incubated with fluorescently labeled secondary antibodies and phalloidin in blocking buffer for 2 hr at room temperature (Alexa Fluor 555-conjugated secondary antibody, Thermo Fisher Scientific, Secondary- Cat# A-31572, Cat# A-31573, Phalloidin- Cat A12379). After secondary antibody incubation, tissues were washed three additional times in PBS, mounted onto glass slides using ProLong Gold Antifade Mounting Media (Thermo Fisher Scientific, P36930), and allowed to cure overnight. Confocal imaging was performed using a Leica Stellaris 5 confocal microscope equipped with a ×63 oil-immersion objective.

ATP8B1-HA fluorescence line scan analysis

Cochleae from *Atp8b1*^{HA} knock-in mice were immunostained with anti-HA antibody and labeled with phalloidin to visualize F-actin as described in the immunofluorescence protocol above. Confocal images were acquired using a Leica Stellaris 5 confocal microscope equipped with a ×63 oil-immersion objective. High-resolution images of outer hair cell stereocilia were collected using identical acquisition parameters across samples. To assess sub-stereociliary localization of ATP8B1-HA, fluorescence intensity line scans were performed along individual stereocilia using ImageJ (NIH). Line scans were drawn manually along the length of both long (row 1) and short (row 2) stereocilia from the base at the cuticular plate to the stereocilia tip. Fluorescence intensity profiles for ATP8B1-HA and phalloidin were extracted and background-subtracted. For each stereocilium, positional distance was normalized from 0 (base) to 1 (tip), and fluorescence intensity was normalized to the total signal per stereocilium to allow comparison across cells. Normalized intensity profiles were averaged across stereocilia, and shaded regions represent the SEM.

Fluorescence intensity quantifications of ATP8B1-HA and TMEM30B-HA

Cochleae were immunostained with anti-HA antibody and labeled with phalloidin as described in the immunofluorescence protocol above. Confocal images were acquired using a Leica Stellaris 5 confocal microscope equipped with a ×63 oil-immersion objective. For each experiment, all images were acquired using identical acquisition parameters, including zoom and laser power, across genotypes within that experiment. Fluorescence intensity of the HA signal was quantified in ImageJ (NIH). Whole-mount images were resliced to generate orthogonal views, and regions of interest (ROIs) were manually drawn around the hair bundle and hair cell soma. Background fluorescence was measured in adjacent regions lacking specific signal and subtracted from all measurements. For all analyses, measurements were restricted to the middle cochlear turn. For each cochlea, fluorescence intensity was measured in five outer hair cells and averaged to generate a single biological replicate (n=4–6 cochleae per genotype, 1 cochlea representing 1 mouse). Data analysis and statistical testing were performed using GraphPad Prism.

Quantitative PCR

qPCR primers were designed to detect ATP8B1 expression levels. Total RNA was extracted using TRIzol reagent (15596026, Thermo Fisher Scientific). Reverse transcription was performed using the SuperScript IV Reverse Transcription system (18090010, Thermo Fisher Scientific). qPCR reactions were conducted using iTaq Universal SYBR Green Supermix (1725121, Bio-Rad, CA, USA) on a CFX Opus 384 Real-Time PCR System (12011319, Bio-Rad) for fluorescence measurement. Transcript level of *Atp8b1* is normalized to the transcript level of *Gapdh*. Expression analysis was performed in GraphPad Prism.

Atp8b1 Primers used were:

Forward: ACGGCCGGTGGTCTTACATA
Reverse: GCTTGTCACTCACGTCCTGAT

Gapdh Primers used were:

Forward: AACGACCCCTTCATTGAC
Reverse: TCCACGACATACTCAGCAC

Hair cell counts

Cochleae were immunostained for MYO7A (Rabbit polyclonal anti-MYO7A, Proteus Biosciences Inc, Ramona, CA, 25–6790) and labeled with phalloidin as described in the immunofluorescence protocol above. Confocal images were acquired using a Leica Stellaris 5 confocal microscope equipped with a ×63 oil-immersion objective. For each experiment, all images were acquired using identical acquisition parameters, including zoom and laser power, across genotypes within that experiment. Hair cells were quantified using the Cell Counter plugin in ImageJ (NIH) based on the presence of MYO7A-positive cells. Counts were performed separately for apical, middle, and basal cochlear turns, defined by their relative position along the cochlear spiral (n=3–5 cochleae per genotype, 1 cochlea representing 1 mouse). Data analysis and statistical testing were performed using GraphPad Prism.

Annexin V staining and quantification

P15 mice were euthanized and cochleae were rapidly dissected and gently opened to facilitate Annexin V penetration. Cochleae were flushed with Alexa Fluor 488–conjugated Annexin V (Thermo Fisher Scientific Cat # A13201) diluted 1:25 (10 µL Annexin V in 250 µL L-15 medium, GIBCO, Thermo Fisher Scientific; total volume ~260 µL) and then incubated for 30 min at room temperature. Following incubation, cochleae were washed twice in L-15 medium, fixed in 4% paraformaldehyde, and washed three times in PBS (5 min each). Samples were then dissected and mounted using ProLong Gold antifade mounting medium. Confocal images were acquired using a Leica Stellaris 5 confocal microscope equipped with a ×63 oil-immersion objective for the *Atp8b1* knockout experiments and a Leica Stellaris 8 confocal microscope for the *Tmem30b* knockout experiments due to instrument availability. For each experiment, all images were acquired using identical acquisition parameters, including zoom and laser power, across genotypes within that experiment. Fluorescence intensity of the Annexin V signal was quantified in ImageJ. ROIs were manually drawn around individual outer hair cells, and mean fluorescence intensity was measured using the ImageJ (NIH) measurement function. Background fluorescence was measured in adjacent regions lacking specific signal and subtracted from all measurements. Analyses were restricted to the apical cochlear turn, as decalcification was not performed prior to Annexin V incubation. For each cochlea, fluorescence intensity was measured in five outer hair cells and averaged to generate a single biological replicate (n=5–7 cochleae per genotype, 1 cochlea representing 1 mouse). Data analysis and statistical testing were performed using GraphPad Prism.

Scanning electron microscopy

Mice were sacrificed via decapitation (P5 and younger) or CO2 asphyxiation followed by cervical dislocation (P6 and older). Cochleae were carefully dissected and placed in a dish containing PBS (GIBCO, Thermo Fisher Scientific). Under a dissecting microscope, ossicles were removed, and the cochleae were transferred to conical tubes containing 2.5% glutaraldehyde and 2% paraformaldehyde (PFA; Electron Microscopy Sciences). Samples were incubated in this fixative solution overnight at 4 °C. For adult mice, cochleae were subsequently incubated in 0.5 M ethylenediaminetetraacetic acid (EDTA; Bioland Scientific LLC), pH 8.0, for up to two weeks to facilitate decalcification, depending on bone density. Following decalcification, the cochleae were further dissected to expose the organ of Corti, ensuring the complete removal of the tectorial membrane. Samples were prepared for SEM using the OTOTO procedure (***Davies and Forge, 1987***). This process included sequential osmium tetroxide and thiocarbohydrazide treatments, followed by dehydration through a graded ethanol series and critical point drying using hexamethyldisilazane (HMDS; Electron Microscopy Services). Once dried, samples were sputter-coated with a thin layer of platinum to enhance conductivity. Imaging was performed on a JEOL JSM-IT710HR InTouchScope Scanning Electron Microscope housed in our microscopy core facility. SEM images were pseudocolored using Affinity (Canva Pty Ltd.)

Hearing tests in mice

Prior to ABR tests, mice were anesthetized with an intraperitoneal injection of 20 mg/kg ketamine hydrochloride (Covetrus Inc) and 10 mg/kg xylazine hydrochloride (Covetrus Inc). ABR tests were performed in a sound isolating cubicle (Med-Associates, product number: ENV-022MD-WF). To maintain body temperature, mice were kept on a Deltaphase isothermal heating pad (Braintree Scientific). ABR recording equipment was purchased from Tucker-Davis Technologies (Alachua, FL). Recordings were captured by subdermal needle electrodes (FE-7; Grass Technologies). The noninverting electrode

was placed at the vertex of the midline, the inverting electrode over the mastoid of the right ear, and the ground electrode on the upper thigh. Stimulus tones (pure tones) were presented at a rate of 21.1 /s through a high-frequency transducer (Tucker-Davis Technologies). Responses were filtered at 300–3000 Hz and threshold levels were determined from 1024 stimulus presentations at 8, 11.3, 16, 22.4, and 32 kHz. Stimulus intensity was decreased in 5–10 dB steps until a response waveform could no longer be identified. Stimulus intensity was then increased in 5 dB steps until a waveform could again be identified. If a waveform could not be identified at the maximum output of the transducer, a value of 5 dB was added to the maximum output as the threshold. DPOAEs of the same group of WT and *Atp8b1* and *Tmem30b* KO mice were recorded. While under anesthesia for ABR testing, DPOAE was recorded using SmartOAE ver. 5.20 (Intelligent Hearing Systems). A range of pure tones from 8 to 32 kHz (16 sweeps) was used to obtain the DPOAE for the right ear. DPOAE recordings were made for f2 frequencies from 8.8 to 35.3 kHz using a paradigm set as follows: L1 = 65 dB, L2 = 55 dB SPL, and f2/f1 = 1.22. Mice were separated by sex when tested for initial ABR and DPOAE experiments. We did not find any significant difference in ABR and DPOAE thresholds based on sex (not shown). ABR analysis for *Atp8b1*^{HA}, *Tmem30b*^{HA}, *Atp8b1* KO, and *Tmem30b* KO mice contain both males and females. DPOAE analysis for *Atp8b1* KO, and *Tmem30b* KO mice contain both males and females.

Statistics and reproducibility

All statistical analyses were performed using GraphPad Prism (GraphPad Software, La Jolla, CA, USA). ABR thresholds were compared between genotypes using Mann–Whitney U tests. For all statistical analyses, significance was defined as $p<0.05$. In figures, statistically significant p-values are indicated, whereas non-significant comparisons are not shown. Unless otherwise indicated, error bars represent standard deviation. Analyses in this study use biological replicates. Experiments were repeated between two and four times. Power analyses were conducted using preliminary means and standard deviations to determine appropriate sample sizes. Based on an effect size of Cohen's d=1.4 calculated from preliminary ABR data, a one-tailed test with α=0.05 and a desired power of 0.8 (80%) indicated that a sample size of 10 mice per group (20 total) was sufficient to detect statistically significant differences between genotypes (***Faul et al., 2007***; ***Faul et al., 2009***). Sample sizes for immunofluorescence experiments (hair cell counts, HA fluorescence intensity, and Annexin V staining) were determined based on prior experience with similar experiments, as the variability between genotypes could not be estimated a priori. Hair-cell counts and Annexin V fluorescence intensity were analyzed using Welch's t-tests.

Acknowledgements

We thank Wenhao Xu and Daniel Grigsby at Genetically Engineered Murine Model Core (University of Virginia, RRID:SCR_025473) for generating mouse models used in this study. We thank Sijie Hao from Advanced Microscopy Facility (University of Virginia, RRID:SCR_018736) for the support of SEM imaging. Graphics were created in Biorender. Funding sources: JBS is supported by NIH grant R01DC018842 and R01DC021176. HND is supported by NIH grant F30DC023139.

Additional information

Funding

Funder	Grant reference number	Author
National Institute on Deafness and Other Communication Disorders	R01DC018842	Jung-Bum Shin
National Institute on Deafness and Other Communication Disorders	R01DC021176	Jung-Bum Shin
National Institute on Deafness and Other Communication Disorders	F30DC023139	Henry Newkirk De Hoyos

Funder	Grant reference number	Author

The funders had no role in study design, data collection and interpretation, or the decision to submit the work for publication.

Author contributions

Henry Newkirk De Hoyos, Conceptualization, Data curation, Formal analysis, Funding acquisition, Validation, Investigation, Visualization, Methodology, Writing – original draft, Project administration, Writing – review and editing; Sihan Li, Conceptualization, Data curation, Validation, Methodology; Jun-Sub Im, Data curation, Formal analysis, Investigation, Methodology; Alyssa Luz-Ricca, Formal analysis, Validation, Investigation, Visualization; Takesha Foster, Data curation, Validation, Investigation; Betsy Szeto, Conceptualization, Formal analysis, Investigation, Methodology; Rachel Jonas, Conceptualization, Resources, Validation; Emma Kim, Nikhil Amin, Validation, Investigation, Methodology; Jung-Bum Shin, Conceptualization, Resources, Data curation, Supervision, Funding acquisition, Investigation, Methodology, Writing – original draft, Project administration, Writing – review and editing

Author ORCIDs

Henry Newkirk De Hoyos https://orcid.org/0000-0002-2083-1261
Sihan Li https://orcid.org/0000-0001-5396-6181
Alyssa Luz-Ricca https://orcid.org/0000-0003-4336-099X
Takesha Foster https://orcid.org/0009-0000-9548-6362
Jung-Bum Shin https://orcid.org/0000-0003-3047-0874

Ethics

All murine experiments conducted for this study adhered to the guidelines established by the University of Virginia Institutional Animal Care and Use Committee (IACUC) and the NIH. Animal protocols were reviewed and approved by the University of Virginia IACUC. Mice were housed in an AAALAC-accredited vivarium located in the basement of our research building. Animals were maintained on a 12-hour light/dark cycle, with cage changes performed every five days. Mice had ad libitum access to standard rodent chow and water provided through lixit systems. Control mice were C57BL/6J mice obtained from Jackson Laboratory. Experimental mice ranged from postnatal day 0 (P0) to P5 and were euthanized via rapid decapitation. Mice aged P6 and older were euthanized using CO2 asphyxiation, followed by cervical dislocation as a secondary method to ensure humane euthanasia.

Peer review material

Version of Record:
Reviewer #1 (Public review): https://doi.org/10.7554/eLife.110466.4.sa1
Reviewer #2 (Public review): https://doi.org/10.7554/eLife.110466.4.sa2
Author response https://doi.org/10.7554/eLife.110466.4.sa3

Reviewed preprint v3
Reviewer #1 (Public review): https://doi.org/10.7554/eLife.110466.3.sa2
Reviewer #2 (Public review): https://doi.org/10.7554/eLife.110466.3.sa1
Author response: https://doi.org/10.7554/eLife.110466.3.sa0
eLife Assessment https://doi.org/10.7554/eLife.110466.3.sa3

Reviewed preprint v2
Reviewer #1 (Public review): https://doi.org/10.7554/eLife.110466.2.sa2
Reviewer #2 (Public review): https://doi.org/10.7554/eLife.110466.2.sa1
Author response: https://doi.org/10.7554/eLife.110466.2.sa0
eLife Assessment https://doi.org/10.7554/eLife.110466.2.sa3

Reviewed preprint v1
Reviewer #1 (Public review): https://doi.org/10.7554/eLife.110466.1.sa2
Reviewer #2 (Public review): https://doi.org/10.7554/eLife.110466.1.sa1
Author Response: https://doi.org/10.7554/eLife.110466.1.sa0
eLife Assessment https://doi.org/10.7554/eLife.110466.1.sa3

Additional files

Supplementary files

MDAR checklist

Data availability

Raw data used to create this manuscript are available on https://doi.org/10.17605/OSF.IO/GQBMF. Mouse lines and other reagents are available from the corresponding author upon request.

The following dataset was generated:

Author(s)	Year	Dataset title	Dataset URL	Database and Identifier
Shin J-B, De Hoyos H	2026	ATP8B1-TMEM30B Flippase Activity Maintains Stereocilia Lipid Asymmetry Required for Hearing	https://doi.org/10.17605/OSF.IO/GQBMF	Open Science Framework, 10.17605/OSF.IO/GQBMF

References

Ahmed ZM, Goodyear R, Riazuddin S, Lagziel A, Legan PK, Behra M, Burgess SM, Lilley KS, Wilcox ER, Riazuddin S, Griffith AJ, Frolenkov GI, Belyantseva IA, Richardson GP, Friedman TB. 2006. The tip-link antigen, a protein associated with the transduction complex of sensory hair cells, is protocadherin-15. *The Journal of Neuroscience* **26**:7022–7034. DOI: https://doi.org/10.1523/JNEUROSCI.1163-06.2006, PMID: 16807332

Assad JA, Shepherd GMG, Corey DP. 1991. Tip-link integrity and mechanical transduction in vertebrate hair cells. *Neuron* **7**:985–994. DOI: https://doi.org/10.1016/0896-6273(91)90343-x, PMID: 1764247

Ballesteros A, Fenollar-Ferrer C, Swartz KJ. 2018. Structural relationship between the putative hair cell mechanotransduction channel TMC1 and TMEM16 proteins. *eLife* **7**:e38433. DOI: https://doi.org/10.7554/eLife.38433, PMID: 30063209

Ballesteros A, Swartz KJ. 2022. Regulation of membrane homeostasis by TMC1 mechanoelectrical transduction channels is essential for hearing. *Science Advances* **8**:eabm5550. DOI: https://doi.org/10.1126/sciadv.abm5550, PMID: 35921424

Beurg M, Konrad DE, Fettiplace R. 2025. Hair cell apoptosis and deafness in Tmc1 mutations. *PNAS* **122**:e2425215122. DOI: https://doi.org/10.1073/pnas.2425215122, PMID: 40100636

Bhandari N, Prince A, Khan MR, Traughber CA, Neupane K, Lorkowski SW, Brubaker G, Ertugral EG, Kothapalli CR, Dubyak GR, Smith JD, Gulshan K. 2025. ATP8B1 regulates PIP2 localization and cleavage of pyroptotic executioner Gasdermin D. *PNAS* **122**:e2502798122. DOI: https://doi.org/10.1073/pnas.2502798122, PMID: 40440066

Blom T, Somerharju P, Ikonen E. 2011. Synthesis and biosynthetic trafficking of membrane lipids. *Cold Spring Harbor Perspectives in Biology* **3**:a004713. DOI: https://doi.org/10.1101/cshperspect.a004713, PMID: 21482741

Bowl MR, Simon MM, Ingham NJ, Greenaway S, Santos L, Cater H, Taylor S, Mason J, Kurbatova N, Pearson S, Bower LR, Clary DA, Meziane H, Reilly P, Minowa O, Kelsey L, Allen S, Clementson-Mobbs S, Codner G, Fray M, et al. 2017. A large scale hearing loss screen reveals an extensive unexplored genetic landscape for auditory dysfunction. *Nature Communications* **8**:886. DOI: https://doi.org/10.1038/s41467-017-00595-4, PMID: 29026089

Bretscher MS. 1972. Asymmetrical lipid bilayer structure for biological membranes. *Nature* **236**:11–12. DOI: https://doi.org/10.1038/newbio236011a0, PMID: 4502419

Bryde S, Hennrich H, Verhulst PM, Devaux PF, Lenoir G, Holthuis JCM. 2010. CDC50 proteins are critical components of the human class-1 P4-ATPase transport machinery. *The Journal of Biological Chemistry* **285**:40562–40572. DOI: https://doi.org/10.1074/jbc.M110.139543, PMID: 20961850

Caputo M, Gubar O, Tóth P, Vitale N, Gasman S, Ory S. 2025. Lipid asymmetry and membrane trafficking: Transbilayer distribution of structural phospholipids as regulators of exocytosis and endocytosis. *The Journal of Biological Chemistry* **301**:110441. DOI: https://doi.org/10.1016/j.jbc.2025.110441, PMID: 40609796

Chang M, Hong G, Gao S, Cheng C, Yuan J, Xiao Y, Qiao R, Ke J, Wu X, Zhang T, Guo S, Jiang R, Liu Z, Zhou J, Zhang X, Wu Y, Zhao X, Li W, Shen S, He Z, et al. 2026. Regulation of Tmem30b-mediated apical membrane homeostasis in auditory outer hair cells is critical for hearing. *PNAS* **123**. DOI: https://doi.org/10.1073/pnas.2531557123

Clark S, Jeong H, Posert R, Goehring A, Gouaux E. 2024. The structure of the *Caenorhabditis elegans* TMC-2 complex suggests roles of lipid-mediated subunit contacts in mechanosensory transduction. *PNAS* **121**:e2314096121. DOI: https://doi.org/10.1073/pnas.2314096121, PMID: 38354260

Coleman JA, Zhu X, Djajadi HR, Molday LL, Smith RS, Libby RT, John SWM, Molday RS. 2014. Phospholipid flippase ATP8A2 is required for normal visual and auditory function and photoreceptor and spiral ganglion cell survival. *Journal of Cell Science* **127**:1138–1149. DOI: https://doi.org/10.1242/jcs.145052, PMID: 24413176

Cooper GM. 2000. Cell membranes. In: Cooper GM (Ed). *The Cell: A Molecular Approach*. Sinauer Associates. p. 79–88.
Corns LF, Johnson SL, Kros CJ, Marcotti W. 2014. Calcium entry into stereocilia drives adaptation of the mechanoelectrical transducer current of mammalian cochlear hair cells. *PNAS* **111**:14918–14923. DOI: https://doi.org/10.1073/pnas.1409920111, PMID: 25228765
Davies S, Forge A. 1987. Preparation of the mammalian organ of Corti for scanning electron microscopy. *Journal of Microscopy* **147**:89–101. DOI: https://doi.org/10.1111/j.1365-2818.1987.tb02821.x, PMID: 3305958
Dieudonné T, Herrera SA, Laursen MJ, Lejeune M, Stock C, Slimani K, Jaxel C, Lyons JA, Montigny C, Pomorski TG, Nissen P, Lenoir G. 2022. Autoinhibition and regulation by phosphoinositides of ATP8B1, a human lipid flippase associated with intrahepatic cholestatic disorders. *eLife* **11**:e75272. DOI: https://doi.org/10.7554/eLife.75272, PMID: 35416773
Dieudonné T, Kümmerer F, Laursen MJ, Stock C, Flygaard RK, Khalid S, Lenoir G, Lyons JA, Lindorff-Larsen K, Nissen P. 2023. Activation and substrate specificity of the human P4-ATPase ATP8B1. *Nature Communications* **14**:7492. DOI: https://doi.org/10.1038/s41467-023-42828-9, PMID: 37980352
Doktorova M, Symons JL, Levental I. 2020. Structural and functional consequences of reversible lipid asymmetry in living membranes. *Nature Chemical Biology* **16**:1321–1330. DOI: https://doi.org/10.1038/s41589-020-00688-0, PMID: 33199908
Faul F, Erdfelder E, Lang AG, Buchner A. 2007. G*Power 3: a flexible statistical power analysis program for the social, behavioral, and biomedical sciences. *Behavior Research Methods* **39**:175–191. DOI: https://doi.org/10.3758/bf03193146, PMID: 17695343
Faul F, Erdfelder E, Buchner A, Lang AG. 2009. Statistical power analyses using G*Power 3.1: tests for correlation and regression analyses. *Behavior Research Methods* **41**:1149–1160. DOI: https://doi.org/10.3758/BRM.41.4.1149, PMID: 19897823
Fettiplace R, Kim KX. 2014. The physiology of mechanoelectrical transduction channels in hearing. *Physiological Reviews* **94**:951–986. DOI: https://doi.org/10.1152/physrev.00038.2013, PMID: 24987009
George SS, Steele CR, Ricci AJ. 2020. Rat auditory inner hair cell mechanotransduction and stereociliary membrane diffusivity are similarly modulated by calcium. *iScience* **23**:101773. DOI: https://doi.org/10.1016/j.isci.2020.101773, PMID: 33294782
George SS, Ricci AJ. 2026. Auditory hair cell mechanotransduction channels dynamically shape the mechanical properties of their membrane environment. *Advanced Science* **13**:e08268. DOI: https://doi.org/10.1002/advs.202508268, PMID: 40908646
Giese APJ, Tang Y-Q, Sinha GP, Bowl MR, Goldring AC, Parker A, Freeman MJ, Brown SDM, Riazuddin S, Fettiplace R, Schafer WR, Frolenkov GI, Ahmed ZM. 2017. CIB2 interacts with TMC1 and TMC2 and is essential for mechanotransduction in auditory hair cells. *Nature Communications* **8**:43. DOI: https://doi.org/10.1038/s41467-017-00061-1, PMID: 28663585
Gillespie PG, Müller U. 2009. Mechanotransduction by hair cells: models, molecules, and mechanisms. *Cell* **139**:33–44. DOI: https://doi.org/10.1016/j.cell.2009.09.010, PMID: 19804752
Gómez-Mellado VE, Chang J-C, Ho-Mok KS, Bernardino Morcillo C, Kersten RHJ, Oude Elferink RPJ, Verhoeven AJ, Paulusma CC. 2022. ATP8B1 deficiency results in elevated mitochondrial phosphatidylethanolamine levels and increased mitochondrial oxidative phosphorylation in human hepatoma cells. *International Journal of Molecular Sciences* **23**:12344. DOI: https://doi.org/10.3390/ijms232012344, PMID: 36293199
Goodyear RJ, Gale JE, Ranatunga KM, Kros CJ, Richardson GP. 2008. Aminoglycoside-induced phosphatidylserine externalization in sensory hair cells is regionally restricted, rapid, and reversible. *The Journal of Neuroscience* **28**:9939–9952. DOI: https://doi.org/10.1523/JNEUROSCI.1124-08.2008, PMID: 18829952
Haeussler M, Schönig K, Eckert H, Eschstruth A, Mianné J, Renaud J-B, Schneider-Maunoury S, Shkumatava A, Teboul L, Kent J, Joly J-S, Concordet J-P. 2016. Evaluation of off-target and on-target scoring algorithms and integration into the guide RNA selection tool CRISPOR. *Genome Biology* **17**:148. DOI: https://doi.org/10.1186/s13059-016-1012-2, PMID: 27380939
Hossein A, Deserno M. 2020. Spontaneous curvature, differential stress, and bending modulus of asymmetric lipid membranes. *Biophysical Journal* **118**:624–642. DOI: https://doi.org/10.1016/j.bpj.2019.11.3398, PMID: 31954503
Hudspeth AJ. 1989. How the ear's works work. *Nature* **341**:397–404. DOI: https://doi.org/10.1038/341397a0, PMID: 2677742
Jeong H, Clark S, Goehring A, Dehghani-Ghahnaviyeh S, Rasouli A, Tajkhorshid E, Gouaux E. 2022. Structures of the TMC-1 complex illuminate mechanosensory transduction. *Nature* **610**:796–803. DOI: https://doi.org/10.1038/s41586-022-05314-8, PMID: 36224384
Johnson SL, Beurg M, Marcotti W, Fettiplace R. 2011. Prestin-driven cochlear amplification is not limited by the outer hair cell membrane time constant. *Neuron* **70**:1143–1154. DOI: https://doi.org/10.1016/j.neuron.2011.04.024, PMID: 21689600
Kakuda S, Suresh P, Li G, London E. 2022. Loss of plasma membrane lipid asymmetry can induce ordered domain (raft) formation. *Journal of Lipid Research* **63**:100155. DOI: https://doi.org/10.1016/j.jlr.2021.100155, PMID: 34843684
Kawashima Y, Géléoc GSG, Kurima K, Labay V, Lelli A, Asai Y, Makishima T, Wu DK, Della Santina CC, Holt JR, Griffith AJ. 2011. Mechanotransduction in mouse inner ear hair cells requires transmembrane channel-like genes. *The Journal of Clinical Investigation* **121**:4796–4809. DOI: https://doi.org/10.1172/JCI60405, PMID: 22105175

Kazmierczak P, Sakaguchi H, Tokita J, Wilson-Kubalek EM, Milligan RA, Müller U, Kachar B. 2007. Cadherin 23 and protocadherin 15 interact to form tip-link filaments in sensory hair cells. *Nature* **449**:87–91. DOI: https://doi.org/10.1038/nature06091, PMID: 17805295

Klomp LWJ, Vargas JC, van Mil SWC, Pawlikowska L, Strautnieks SS, van Eijk MJT, Juijn JA, Pabón-Peña C, Smith LB, DeYoung JA, Byrne JA, Gombert J, van der Brugge G, Berger R, Jankowska I, Pawlowska J, Villa E, Knisely AS, Thompson RJ, Freimer NB, et al. 2004. Characterization of mutations in ATP8B1 associated with hereditary cholestasis. *Hepatology* **40**:27–38. DOI: https://doi.org/10.1002/hep.20285, PMID: 15239083

Kolla L, Kelly MC, Mann ZF, Anaya-Rocha A, Ellis K, Lemons A, Palermo AT, So KS, Mays JC, Orvis J, Burns JC, Hertzano R, Driver EC, Kelley MW. 2020. Characterization of the development of the mouse cochlear epithelium at the single cell level. *Nature Communications* **11**:2389. DOI: https://doi.org/10.1038/s41467-020-16113-y, PMID: 32404924

Koopman G, Reutelingsperger CP, Kuijten GA, Keehnen RM, Pals ST, van Oers MH. 1994. Annexin V for flow cytometric detection of phosphatidylserine expression on B cells undergoing apoptosis. *Blood* **84**:1415–1420 PMID: 8068938.

Kozel PJ, Friedman RA, Erway LC, Yamoah EN, Liu LH, Riddle T, Duffy JJ, Doetschman T, Miller ML, Cardell EL, Shull GE. 1998. Balance and hearing deficits in mice with a null mutation in the gene encoding plasma membrane Ca2+-ATPase isoform 2. *The Journal of Biological Chemistry* **273**:18693–18696. DOI: https://doi.org/10.1074/jbc.273.30.18693, PMID: 9668038

Le SC, Yang H. 2021. Structure-function of TMEM16 ion channels and lipid scramblases. *Advances in Experimental Medicine and Biology* **1349**:87–109. DOI: https://doi.org/10.1007/978-981-16-4254-8_6, PMID: 35138612

Lenoir G, Williamson P, Puts CF, Holthuis JCM. 2009. Cdc50p plays a vital role in the ATPase reaction cycle of the putative aminophospholipid transporter Drs2p. *The Journal of Biological Chemistry* **284**:17956–17967. DOI: https://doi.org/10.1074/jbc.M109.013722, PMID: 19411703

Li T, Yu D, Oak HC, Zhu B, Wang L, Jiang X, Molday RS, Kriegstein A, Piao X. 2021. Phospholipid-flippase chaperone CDC50A is required for synapse maintenance by regulating phosphatidylserine exposure. *The EMBO Journal* **40**:e107915. DOI: https://doi.org/10.15252/embj.2021107915, PMID: 34585770

Li X, Li S, Zhang W, Wang Q, Zou W. 2024. Impacts of P4-ATPase deletion on membrane asymmetry and disease development. *Cell Biochemistry and Function* **42**:e70004. DOI: https://doi.org/10.1002/cbf.70004, PMID: 39425455

Liu H, Chen L, Giffen KP, Stringham ST, Li Y, Judge PD, Beisel KW, He DZZ. 2018. Cell-specific transcriptome analysis shows that adult pillar and deiters' cells express genes encoding machinery for specializations of cochlear hair cells. *Frontiers in Molecular Neuroscience* **11**:356. DOI: https://doi.org/10.3389/fnmol.2018.00356, PMID: 30327589

Lorent JH, Levental KR, Ganesan L, Rivera-Longsworth G, Sezgin E, Doktorova M, Lyman E, Levental I. 2020. Plasma membranes are asymmetric in lipid unsaturation, packing and protein shape. *Nature Chemical Biology* **16**:644–652. DOI: https://doi.org/10.1038/s41589-020-0529-6, PMID: 32367017

Medrano-Soto A, Moreno-Hagelsieb G, McLaughlin D, Ye ZS, Hendargo KJ, Saier MH. 2018. Bioinformatic characterization of the Anoctamin Superfamily of Ca2+-activated ion channels and lipid scramblases. *PLOS ONE* **13**:e0192851. DOI: https://doi.org/10.1371/journal.pone.0192851, PMID: 29579047

Nagata S, Hanayama R, Kawane K. 2010. Autoimmunity and the clearance of dead cells. *Cell* **140**:619–630. DOI: https://doi.org/10.1016/j.cell.2010.02.014, PMID: 20211132

Nagata S, Sakuragi T, Segawa K. 2020. Flippase and scramblase for phosphatidylserine exposure. *Current Opinion in Immunology* **62**:31–38. DOI: https://doi.org/10.1016/j.coi.2019.11.009, PMID: 31837595

Orvis J, Gottfried B, Kancherla J, Adkins RS, Song Y, Dror AA, Olley D, Rose K, Chrysostomou E, Kelly MC, Milon B, Matern MS, Azaiez H, Herb B, Colantuoni C, Carter RL, Ament SA, Kelley MW, White O, Bravo HC, et al. 2021. gEAR: Gene Expression Analysis Resource portal for community-driven, multi-omic data exploration. *Nature Methods* **18**:843–844. DOI: https://doi.org/10.1038/s41592-021-01200-9, PMID: 34172972

Osada N, Hashimoto K, Hirai M, Kusuda J. 2007. Aberrant termination of reproduction-related TMEM30C transcripts in the hominoids. *Gene* **392**:151–156. DOI: https://doi.org/10.1016/j.gene.2006.11.021, PMID: 17258408

Pan B, Géléoc GS, Asai Y, Horwitz GC, Kurima K, Ishikawa K, Kawashima Y, Griffith AJ, Holt JR. 2013. TMC1 and TMC2 are components of the mechanotransduction channel in hair cells of the mammalian inner ear. *Neuron* **79**:504–515. DOI: https://doi.org/10.1016/j.neuron.2013.06.019, PMID: 23871232

Pan B, Akyuz N, Liu X-P, Asai Y, Nist-Lund C, Kurima K, Derfler BH, György B, Limapichat W, Walujkar S, Wimalasena LN, Sotomayor M, Corey DP, Holt JR. 2018. TMC1 forms the pore of mechanosensory transduction channels in vertebrate inner ear hair cells. *Neuron* **99**:736–753.. DOI: https://doi.org/10.1016/j.neuron.2018.07.033, PMID: 30138589

Pater JA, Penney C, O'Rielly DD, Griffin A, Kamal L, Brownstein Z, Vona B, Vinkler C, Shohat M, Barel O, French CR, Singh S, Werdyani S, Burt T, Abdelfatah N, Houston J, Doucette LP, Squires J, Glaser F, Roslin NM, et al. 2022. Autosomal dominant non-syndromic hearing loss maps to DFNA33 (13q34) and co-segregates with splice and frameshift variants in ATP11A, a phospholipid flippase gene. *Human Genetics* **141**:431–444. DOI: https://doi.org/10.1007/s00439-022-02444-x, PMID: 35278131

Peineau T, Marcovich I, Rodriguez C, O'Malley S, Cui R, Ballesteros A, Holt JR. 2025. Mammalian TMC1 or 2 are necessary for scramblase activity in auditory hair cells. *Hearing Research* **460**:109229. DOI: https://doi.org/10.1016/j.heares.2025.109229, PMID: 40073458

Peng AW, Effertz T, Ricci AJ. 2013. Adaptation of mammalian auditory hair cell mechanotransduction is independent of calcium entry. *Neuron* **80**:960–972. DOI: https://doi.org/10.1016/j.neuron.2013.08.025, PMID: 24267652

Pickles JO, Comis SD, Osborne MP. 1984. Cross-links between stereocilia in the guinea pig organ of Corti, and their possible relation to sensory transduction. *Hearing Research* **15**:103–112. DOI: https://doi.org/10.1016/0378-5955(84)90041-8, PMID: 6436216

Reddy AS, Warshaviak DT, Chachisvilis M. 2012. Effect of membrane tension on the physical properties of DOPC lipid bilayer membrane. *Biochimica et Biophysica Acta - Biomembranes* **1818**:2271–2281. DOI: https://doi.org/10.1016/j.bbamem.2012.05.006, PMID: 22588133

Riazuddin S, Belyantseva IA, Giese APJ, Lee K, Indzhykulian AA, Nandamuri SP, Yousaf R, Sinha GP, Lee S, Terrell D, Hegde RS, Ali RA, Anwar S, Andrade-Elizondo PB, Sirmaci A, Parise LV, Basit S, Wali A, Ayub M, Ansar M, et al. 2012. Alterations of the CIB2 calcium- and integrin-binding protein cause Usher syndrome type 1J and nonsyndromic deafness DFNB48. *Nature Genetics* **44**:1265–1271. DOI: https://doi.org/10.1038/ng.2426, PMID: 23023331

Sam George S, El Bahloul-Jaziri A, Ricci AJ. 2023. Tmc regulates membrane viscosity in mammalian cochlear hair cells. *Biophysical Journal* **122**:91a. DOI: https://doi.org/10.1016/j.bpj.2022.11.692

Scheffer DI, Shen J, Corey DP, Chen Z-Y. 2015. Gene expression by mouse inner ear hair cells during development. *The Journal of Neuroscience* **35**:6366–6380. DOI: https://doi.org/10.1523/JNEUROSCI.5126-14.2015, PMID: 25904789

Segawa K, Kurata S, Nagata S. 2016. Human type IV P-type ATPases that work as plasma membrane phospholipid flippases and their regulation by caspase and calcium. *The Journal of Biological Chemistry* **291**:762–772. DOI: https://doi.org/10.1074/jbc.M115.690727, PMID: 26567335

Segawa K, Kurata S, Nagata S. 2018. The CDC50A extracellular domain is required for forming a functional complex with and chaperoning phospholipid flippases to the plasma membrane. *The Journal of Biological Chemistry* **293**:2172–2182. DOI: https://doi.org/10.1074/jbc.RA117.000289, PMID: 29276178

Shi X, Gillespie PG, Nuttall AL. 2007. Apical phosphatidylserine externalization in auditory hair cells. *Molecular Membrane Biology* **24**:16–27. DOI: https://doi.org/10.1080/09687860600926883, PMID: 17453410

Shin H-W, Takatsu H. 2020. Phosphatidylserine exposure in living cells. *Critical Reviews in Biochemistry and Molecular Biology* **55**:166–178. DOI: https://doi.org/10.1080/10409238.2020.1758624, PMID: 32408772

Shin H-W, Takatsu H. 2025. Substrates, regulation, cellular functions, and disease associations of P4-ATPases. *Communications Biology* **8**:135. DOI: https://doi.org/10.1038/s42003-025-07549-3, PMID: 39875509

Siemens J, Lillo C, Dumont RA, Reynolds A, Williams DS, Gillespie PG, Müller U. 2004. Cadherin 23 is a component of the tip link in hair-cell stereocilia. *Nature* **428**:950–955. DOI: https://doi.org/10.1038/nature02483, PMID: 15057245

Stapelbroek JM, Peters TA, van Beurden DHA, Curfs JHAJ, Joosten A, Beynon AJ, van Leeuwen BM, van der Velden LM, Bull L, Oude Elferink RP, van Zanten BA, Klomp LWJ, Houwen RHJ. 2009. ATP8B1 is essential for maintaining normal hearing. *PNAS* **106**:9709–9714. DOI: https://doi.org/10.1073/pnas.0807919106, PMID: 19478059

Street VA, McKee-Johnson JW, Fonseca RC, Tempel BL, Noben-Trauth K. 1998. Mutations in a plasma membrane Ca2+-ATPase gene cause deafness in deafwaddler mice. *Nature Genetics* **19**:390–394. DOI: https://doi.org/10.1038/1284, PMID: 9697703

Suzuki J, Umeda M, Sims PJ, Nagata S. 2010. Calcium-dependent phospholipid scrambling by TMEM16F. *Nature* **468**:834–838. DOI: https://doi.org/10.1038/nature09583, PMID: 21107324

Takatsu H, Tanaka G, Segawa K, Suzuki J, Nagata S, Nakayama K, Shin HW. 2014. Phospholipid flippase activities and substrate specificities of human type IV P-type ATPases localized to the plasma membrane. *The Journal of Biological Chemistry* **289**:33543–33556. DOI: https://doi.org/10.1074/jbc.M114.593012, PMID: 25315773

van der Mark VA, Elferink RPJO, Paulusma CC. 2013. P4 ATPases: flippases in health and disease. *International Journal of Molecular Sciences* **14**:7897–7922. DOI: https://doi.org/10.3390/ijms14047897, PMID: 23579954

van der Velden LM, Wichers CGK, van Breevoort AED, Coleman JA, Molday RS, Berger R, Klomp LWJ, van de Graaf SFJ. 2010. Heteromeric interactions required for abundance and subcellular localization of human CDC50 proteins and class 1 P4-ATPases. *The Journal of Biological Chemistry* **285**:40088–40096. DOI: https://doi.org/10.1074/jbc.M110.139006, PMID: 20947505

Wang HY, Rumin A, Doktorova M, Sputay D, Chan SH, Wehman AM, Levental KR, Levental I. 2025. Loss of lipid asymmetry facilitates plasma membrane blebbing by decreasing membrane lipid packing. *PNAS* **122**:e2417145122. DOI: https://doi.org/10.1073/pnas.2417145122, PMID: 40324083

Whitlock JM, Chernomordik LV. 2021. Flagging fusion: Phosphatidylserine signaling in cell-cell fusion. *The Journal of Biological Chemistry* **296**:100411. DOI: https://doi.org/10.1016/j.jbc.2021.100411, PMID: 33581114

Xing Y, Peng K, Yi Q, Yu D, Shi H, Yang G, Yin S. 2023. TMEM30A is essential for hair cell polarity maintenance in postnatal mouse cochlea. *Cellular & Molecular Biology Letters* **28**:23. DOI: https://doi.org/10.1186/s11658-023-00437-w, PMID: 36959542

Xiong W, Grillet N, Elledge HM, Wagner TFJ, Zhao B, Johnson KR, Kazmierczak P, Müller U. 2012. TMHS is an integral component of the mechanotransduction machinery of cochlear hair cells. *Cell* **151**:1283–1295. DOI: https://doi.org/10.1016/j.cell.2012.10.041, PMID: 23217710

Zhang G, Gurtu V, Kain SR, Yan G. 1997. Early detection of apoptosis using a fluorescent conjugate of annexin V. *BioTechniques* **23**:525–531. DOI: https://doi.org/10.2144/97233pf01, PMID: 9298227

Zhang J, Xiao P, Zhang X. 2009. Phosphatidylserine externalization in caveolae inhibits Ca2+ efflux through plasma membrane Ca2+-ATPase in ECV304. *Cell Calcium* **45**:177–184. DOI: https://doi.org/10.1016/j.ceca.2008.09.002, PMID: 18929409

Zhao B, Wu Z, Grillet N, Yan L, Xiong W, Harkins-Perry S, Müller U. 2014. TMIE is an essential component of the mechanotransduction machinery of cochlear hair cells. *Neuron* **84**:954–967. DOI: https://doi.org/10.1016/j.neuron.2014.10.041, PMID: 25467981